

Chemical modeling for predicting the abundances of certain aldimines and amines in hot cores

MILAN SIL,¹ PRASANTA GORAI,¹ ANKAN DAS,¹ BRATATI BHAT,¹ EMMANUEL E. ETIM,² AND SANDIP K. CHAKRABARTI^{3,1}

¹Indian Centre for Space Physics, 43, Chalantika, Garia Station Road, Kolkata 700084, India

²Department of Chemical Sciences, Federal University Wukari, Katsina-Ala Road, P.M.B. 1020 Wukari, Taraba State, Nigeria

³S. N. Bose National Centre for Basic Sciences, Salt Lake, Kolkata 700098, India

(Received 2017 July 10; Revised 2017 October 12; Accepted 2017 October 27)

Submitted to ApJ

ABSTRACT

We consider six isomeric groups (CH₃N, CH₅N, C₂H₅N, C₂H₇N, C₃H₇N and C₃H₉N) to review the presence of amines and aldimines within the interstellar medium (ISM). Each of these groups contains at least one aldimine or amine. Methanimine (CH₂NH) from CH₃N and methylamine (CH₃NH₂) from CH₅N isomeric group were detected a few decades ago. Recently, the presence of ethanimine (CH₃CHNH) from C₂H₅N isomeric group has been discovered in the ISM. This prompted us to investigate the possibility of detecting any aldimine or amine from the very next three isomeric groups in this sequence: C₂H₇N, C₃H₇N and C₃H₉N. We employ high-level quantum chemical calculations to estimate accurate energies of all the species. According to enthalpies of formation, optimized energies, and expected intensity ratio, we found that ethylamine (precursor of glycine) from C₂H₇N isomeric group, (1Z)-1-propanimine from C₃H₇N isomeric group, and trimethylamine from C₃H₉N isomeric group are the most viable candidates for the future astronomical detection. Based on our quantum chemical calculations and from other approximations (from prevailing similar types of reactions), a complete set of reaction pathways to the synthesis of ethylamine and (1Z)-1-propanimine is prepared. Moreover, a large gas-grain chemical model is employed to study the presence of these species in the ISM. Our modeling results suggest that ethylamine and (1Z)-1-propanimine could efficiently be formed in hot-core regions and could be observed with present astronomical facilities. Radiative transfer modeling is also implemented to additionally aid their discovery in interstellar space.

Keywords: astrochemistry – dust, extinction – evolution – ISM: abundances – ISM: molecules – methods: numerical

Supproting materials: tar.gz files

1. INTRODUCTION

Almost 200 species have been discovered in the interstellar medium (ISM) or circumstellar shells and most of them are organic in nature (<https://www.astro.uni-koeln.de/cdms/molecules>). The presence of numerous complex organic molecules in the ISM has been reported earlier (Herbst 2006; Cronin & Chang 1993). The chemical richness of extraterrestrial media points to the formation of biomolecules in the ISM. There are some studies on the formation of complex

pre-biotic molecules in collapsing clouds and star-forming regions (Garrod 2013; Chakrabarti & Chakrabarti 2000a,b; Chakrabarti et al. 2015). It is suggested that if the abundance of bio-molecules is too small for detection, their precursors may be observed for estimating the abundances of these bio-molecules (Majumdar et al. 2012, 2013). Aldimines and amines are the building blocks of amino acids (Godfrey et al. 1973; Holtom et al. 2005). Thus the discovery of these species under astrophysical circumstances could be treated as important clues leading to the origin of life.

Aldimines are very important as they are seen within the reactions of Strecker-type synthesis. The Strecker synthesis prepares α -aminonitriles, which are versatile intermediates for the synthesis of amino acids via hydrolysis of nitriles.

However, a Strecker-type formation route was found to be less important (Elsila et al. 2007). Therefore, we investigate a total of 34 molecules from six isomeric groups namely, CH_3N , CH_5N , $\text{C}_2\text{H}_5\text{N}$, $\text{C}_2\text{H}_7\text{N}$, $\text{C}_3\text{H}_7\text{N}$ and $\text{C}_3\text{H}_9\text{N}$ to find out the possibility of detecting some of the aldimines and amines which are the precursor of amino acids. From these six isomeric groups, at least one species was observed from each of the CH_3N , CH_5N and $\text{C}_2\text{H}_5\text{N}$ isomeric groups. However, to date, any species from the $\text{C}_2\text{H}_7\text{N}$, $\text{C}_3\text{H}_7\text{N}$ and $\text{C}_3\text{H}_9\text{N}$ isomeric groups is yet to be detected.

From the CH_3N isomeric group, methanimine (CH_2NH) was observed in Sgr B2 (Godfrey et al. 1973). The simplest amino acid, namely, glycine could have been formed by the reaction between methanimine and formic acid (Godfrey et al. 1973). In that sense, methanimine is the precursor molecule for glycine (Suzuki et al. 2016). Similarly, from the CH_5N isomeric group, methylamine (CH_3NH_2) was detected (Kaifu et al. 1974; Fourikis et al. 1974) in both Sgr B2 and Orion A. Holtom et al. (2005) showed from theoretical and experimental studies that glycine could have been formed by the reaction with another precursor molecule (reaction between methylamine and CO_2 under UV irradiation on an icy grain mantle). On the other hand, methylamine could be produced by two successive hydrogen addition reactions with methanimine. It can also be formed by four successive hydrogen additions to HCN on the surface of grains (Godfrey et al. 1973; Woon 2002; Theule et al. 2011). Both the precursor molecules (methylamine and ethylamine) of glycine were observed in comet wild 2 (Glavin et al. 2008) and in the coma of 67P/Churyumov-Gerasimenko (by the Rosetta Orbiter Spectrometer for Ion and Neutral Analysis mass spectrometer (Altwegg et al. 2016)).

Microwave and mm-wave spectra of the two conformers of ethanimine (E- and Z-ethanimine) were characterized in order to guide the astronomical searches (Lovas et al. 1980; Brown et al. 1980). They recommended that ethanimine from the $\text{C}_2\text{H}_5\text{N}$ isomeric group should be a possible interstellar molecule which can be seen in space. Finally, ethanimine has been detected with both the forms in the same sources where methanimine has already been observed (Loomis et al. 2013).

From the $\text{C}_2\text{H}_7\text{N}$, $\text{C}_3\text{H}_7\text{N}$ and $\text{C}_3\text{H}_9\text{N}$ isomeric groups, ethylamine, propanimine and trimethylamine are of special interests because they could possibly play a role towards the formation of amino acids and other pre-biotic molecules. Recently, Margulès et al. (2015) has performed the first spectroscopic study of propanimine molecule. Similar to the ethanimine molecule, Margulès et al. (2015) found that propanimine can exist in two conformations, E-propanimine and Z-propanimine. In order to detect these species under astrophysical conditions, the spectroscopic details as well as the chemical abundances of these species are essential to know.

Section 2 describes the computational details and methodology of our work. Results are extensively discussed in Section 3. General conclusions of this work are provided in Section 4. In the Appendix, we present the gas phase formation and destruction pathways. As the supplementary materials of this work, we provide the catalog files for ethylamine and (1Z)-1-propanimine which could be very useful for the future detection of these species in the ISM.

2. COMPUTATIONAL DETAILS AND METHODOLOGY

2.1. Quantum chemical calculations

All the calculations are performed with the Gaussian 09 suite of programs (Frisch et al. 2013). Table 1 shows some ice phase reactions which lead to the formation of various interstellar amines and aldimines. Some of these reactions are radical-radical (RR) in nature and thus can happen at each encounter. However, there are some reactions between neutrals and radicals (NR) which often possess activation barriers. The QST2 method with B3LYP/6-311++G(d,p) levels of theory are employed to calculate various energy barriers (activation barrier and Gibbs free energy of activation). Moreover, QST2 method is also used to determine reaction pathways and transition state structures.

In order to estimate accurate enthalpies of formation of all the species of various isomeric groups, the Gaussian G4 composite method is used. In arriving at an accurate total energy for a given species, the G4 composite method performs a sequence of well-defined ab-initio molecular calculations (Curtiss et al. 2007; Etim et al. 2016). Each fully optimized structure is verified to be a stationary point (having non-negative frequency) by harmonic vibrational frequency calculations. For computing the enthalpy of formation, we calculate atomization energy of molecules. Experimental values of the enthalpy of formation of atoms are taken from Curtiss et al. (1997). In Table 2, we summarize the present astronomical status and enthalpy of formation ($\Delta_f H^0$) of all the species considered here. Subsequently, in all the tables, we arrange the species according to the ascending order of the enthalpy of formation. Some experimental values of the enthalpy of formation (if available) are also shown for comparison. Relative energies of each isomeric group members are also shown with G4 level of theory. Osmont et al. (2007) found that this level of theory is also suitable for the computation of the enthalpies of formation. Moreover, in Table 2, we also include our calculated enthalpies of formation with the B3LYP/6-31G(d,p) level of theory. In our case, we found that the calculated enthalpies of formation with B3LYP/6-31G(d,p) level of theory are closer to the experimentally obtained values than that of the G4 composite method.

Species with permanent electric dipole moments are generally detected from their rotational transitions and about 80% of all the known interstellar and circumstellar molecules were

Table 1. Ice phase formation pathways.

Reaction number (type)	Reactions	Activation barrier (K)
R1(RR) ^a	N + CH ₃ → CH ₂ NH	0.0
R2(RR) ^a	NH + CH ₂ → CH ₂ NH	0.0
R3(RR) ^a	NH ₂ + CH → CH ₂ NH	0.0
R4(NR) ^a	HCN + H → H ₂ CN	3647 ^e
R5(NR) ^a	HCN + H → HCNH	6440 ^e
R6(RR) ^a	H ₂ CN + H → CH ₂ NH	0.0
R7(RR) ^a	HCNH + H → CH ₂ NH	0.0
R8(NR) ^a	CH ₂ NH + H → CH ₃ NH	2134 ^e
R9(NR) ^a	CH ₂ NH + H → CH ₂ NH ₂	3170 ^e
R10(RR) ^a	CH ₃ NH + H → CH ₃ NH ₂	0.0
R11(RR) ^a	CH ₂ NH ₂ + H → CH ₃ NH ₂	0.0
R12(RR) ^b	CH ₂ CN + H → CH ₃ CN	0.0
R13(RR) ^c	CH ₃ + CN → CH ₃ CN	0.0
R14(NR) ^d	CH ₃ CN + H → CH ₃ CNH	1400 ^e
R15(RR) ^d	CH ₃ CNH + H → CH ₃ CHNH	0.0
R16(RR) ^d	CH ₃ + H ₂ CN → CH ₃ CHNH	0.0
R17(NR)	CH ₃ CHNH + H → CH ₃ CH ₂ NH	1846
R18(RR)	CH ₃ CH ₂ NH + H → CH ₃ CH ₂ NH ₂	0.0
R19(RR)	C ₂ H ₅ + H ₂ CN → CH ₃ CH ₂ CHNH	0.0
R20(RR)	C ₂ H ₅ + CN → CH ₃ CH ₂ CN	0.0
R21(NR)	CH ₃ CH ₂ CN + H → CH ₃ CH ₂ CNH	2712
R22(RR)	CH ₃ CH ₂ CNH + H → CH ₃ CH ₂ CHNH	0.0

NOTE—^a Suzuki et al. (2016), ^b Hasegawa, Herbst & Leung (1992), ^c Quan et al. (2010), ^d Quan et al. (2016), ^e Woon (2002).

discovered by these transitions. Intensity of any rotational transition is especially dependent on the temperature and the components (a-type, b-type and c-type) of dipole moment (McMillan et al. 2014; Fortman et al. 2014). Relative signs of the dipole moment components may cause the change of intensities of some transitions (Müller et al. 2016). These intensities are directly proportional to the square of the dipole moment and inversely proportional to the rotational partition function. Thus, in general, for a fixed temperature, higher the dipole moments, intensities are higher. All the molecules considered here have a non-zero permanent electric dipole moment. Dipole moment components along the inertial axis (μ_a , μ_b and μ_c) are summarized in Table 3. We use input and principal axis orientation geometry defined according to the Pickett program to provide the dipole moment components. Since the derived expected intensity ratio relies on the total dipole moment, it remains the same for optimized geometry. For the computation of the dipole moment components, we use various levels of theory. Among them, our calculations at the HF level, yielded excellent agreement with the existing experimental results. Lakard (2003) already analyzed permanent electric dipole moments of some aliphatic primary amines. They used various models for comparing their calculated results with the experimentally obtained results. They found that HF/6-31G(3df) model is more reliable for the aliphatic amines. According to their calculations, on an average, this model can predict values of permanent elec-

tric dipole moments with a deviation of only 2.1% of its experimental values. With reference to their results, here, we use the same method and the basis set to compute the dipole moment components. In Table 3, we show our calculated dipole moment components along with the experimental values, whenever available. Table 3 depicts that for most of the cases our estimated total dipole moments are in good agreement with the experimentally available data. In case of E-Ethanamine of C₂H₅N isomeric group, we found a maximum deviation of (11.5%) between our calculated and experimental values of total dipole moments. On an average, we found a 5.35% deviation between our calculated and experimental.

As mentioned earlier, the rotational spectroscopy is the most convenient as well as the most reliable method for detecting molecules in the ISM. Quantum chemical studies have succeeded in providing reliable spectroscopic constants to aid laboratory microwave studies. Accurate quantum chemical studies of rotational transition frequencies may lead to interstellar detections with confidence. Calculations of the rotational level need high-level basis sets for accurate estimations of structure, spectrum and for optimization to obtain the ground state energy. We use MP2 perturbation method with 6-311++G(d,p) basis set which is capable of producing spectroscopic constants close to the experimental values. Corrections for the interaction between rotational motion and vibrational motion along with corrections for vibrational averaging and anharmonic corrections to the

vibrational motion are also considered in our calculations. In Table 4, we summarize our calculated theoretical values of rotational constants for all the species considered here. A comparison with the existing experimental results, whenever available is also made. These spectroscopic constants can be used to generate catalog files of spectroscopic frequencies by using the SPCAT program (Pickett 1991) in the JPL/CDMS format. Table 4 also contains the rotational partition function of a temperature relevant to the hot core condition (~ 200 K). Among all the species considered here, λ^1 -azanylmethane is a prolate symmetric top and trimethylamine is an oblate symmetric top and both have 3 rotational symmetries. Rest of the species in this study are asymmetric top having rotational symmetry 1. We calculate the rotational partition function for the asymmetric top species by,

$$Q_{rot} = 5.3311 \times 10^6 \sqrt{(T^3/ABC)}/\sigma,$$

where, σ is the rotational symmetry number. Rotational partition function for the prolate symmetric top molecule is calculated by,

$$Q_{rot} = 5.3311 \times 10^6 \sqrt{(T^3/B^2A)}/\sigma.$$

For the oblate symmetric top molecule, rotational partition function is calculated as,

$$Q_{rot} = 5.3311 \times 10^6 \sqrt{(T^3/A^2C)}/\sigma.$$

2.2. Chemical modeling

Our large gas-grain chemical model (Das et al. 2008b, 2013a,b; Majumdar et al. 2014a,b; Das et al. 2015a,b; Gorai et al. 2017a,b) is employed for the purpose of chemical modeling. We assume that gas and grains are coupled through accretion and thermal/non-thermal desorption. Unless otherwise stated, a moderate value of the non-thermal desorption factor ~ 0.03 is assumed as mentioned in Garrod, Wakelam & Herbst (2007). A visual extinction of 150 and a cosmic ray ionization rate of $1.3 \times 10^{-17} \text{ s}^{-1}$ are used. The initial condition is adopted from Leung, Herbst & Huebner (1984). In order to mimic actual physical conditions of the star-forming region, we consider the warm-up method that was established by Garrod & Herbst (2006). Initially, we assume that the cloud remains in isothermal ($T = 10$ K) phase for 10^6 years which is then followed by a subsequent warm-up phase where the temperature can gradually increase up to 200 K in 10^5 years. So, our simulation time is restricted to 1.1×10^6 years. We assume that each phase has the same constant density ($n_H = 10^7 \text{ cm}^{-3}$).

Our gas phase chemical network is principally adopted from the UMIST 2012 database (McElroy et al. 2013). For the grain surface reaction network, we primarily follow Ruaud et al. (2016). In addition to the above network, our network includes some reactions which are needed for the

formation/destruction of interstellar amines and aldimines. Ice phase formation of some of these amines and aldimines which are considered here are shown in Table 1. Similar pathways are also considered for the formation of these species in the gas phase as well.

For the computation of the gas phase rate coefficients of some additional gas phase neutral-radical (NR) reactions with barrier, we use transition state theory (TST), which leads to the Eyring equation (Eyring 1935):

$$k = (K_B T/hc) \exp(-\Delta G^\ddagger/RT) s^{-1}, \quad (1)$$

where, ΔG^\ddagger is the Gibbs free energy of activation and ‘c’ is the concentration which is set to 1. ΔG^\ddagger is calculated by the quantum chemical calculation (QST2 method with B3LYP/6-311++G(d,p)). Equation 1 depicts that rate coefficient is exponentially increasing with the temperature. Thus, to avoid any unattainable rate coefficient around the high temperature domain, we use an upper limit ($10^{-10} \text{ cm}^3 \text{ s}^{-1}$) for Eqn. 1.

Normally, radical-radical addition reaction with a single product can occur through the radiative association. Vasyunin & Herbst (2013) outlined the rate coefficient for the formation of larger molecules by gas phase radiative association reactions. According to them, a larger molecule such as, CH_3OCH_3 can be formed by,



They considered the following temperature dependent rate coefficient for the above reaction:

$$k = 10^{-15} (T/300)^{-3}.$$

In our work, we also consider similar rate coefficients for the radical-radical gas phase reactions leading to a single product. In our model, we consider the formation and destruction of these species in both the phases.

To compute the rate coefficients of ice phase reaction pathways, we use diffusive reactions with a barrier against diffusion ($\kappa \times R_{diff}$) which is based on thermal diffusion (Hasegawa, Herbst & Leung 1992). κ is the quantum mechanical probability of tunneling through a rectangular barrier of thickness d . κ is unity in the absence of a barrier. For reactions with activation energy barriers (E_a), κ is defined as the quantum mechanical probability for tunneling through the rectangular barrier of thickness d ($= 1 \text{ \AA}$) and is calculated by

$$\kappa = \exp[-2(d/\hbar)(2\mu E_a)^{1/2}]. \quad (2)$$

Chemical enrichment of interstellar grain mantles depends on the desorption energies (E_d) and barriers against diffusion (E_b) of the adsorbed species. In the low-temperature regime, the mobility of the lighter species such as, H, D, N and O mainly controls the chemical composition of interstellar grain mantle. Composition of the grain mantle under the

low-temperature regime is already discussed on several occasions (Chakrabarti et al. 2006a,b; Das et al. 2008a, 2010; Das & Chakrabarti 2011; Sahu et al. 2015; Das et al. 2016; Sil et al. 2017). Here, we use $E_b = 0.50E_d$ (Garrod 2013). Binding energies are mostly taken from KIDA database. Binding energy of some of the newly added ice phase species were not available in KIDA database. For these species, we have added the binding energies of the reactants which are required towards the formation of these species. A similar technique was also employed in Garrod (2013). For example, for the calculation of the binding energy of CH_3CNH , we add the binding energies of CH_3CN and H.

For the destruction of gaseous amines and aldimines, we assume various ion-neutral (IN) and photo-dissociative pathways. Various IN and photo-dissociative destruction pathways were already available in Quan et al. (2016) (for ethanimine) and McElroy et al. (2013) (for methanimine). We follow similar pathways and the same rate coefficients for the destructions of other amines, aldimines and their associated species. In the Appendix, we point out all the gas phase formation and destruction reactions which are considered here. In analogy, for the destruction of ice phase amines, aldimines and their associated neutrals, we assume similar photo-dissociative reactions. Rate coefficients for the photo-dissociative reactions are assumed to be the same in both the phases. Abundances of the gas phase species can also decrease via adsorption onto the ice. However, the reverse process of desorption also occurs.

3. RESULTS AND DISCUSSIONS

In this Section, the results of high-level quantum chemical calculations together with our chemical model are presented and discussed. A detailed discussion of each isomeric group is given below.

3.1. CH_3N Isomeric Group

This group contains two molecular species (Figure 1), methanimine and λ^1 -azanylmethane. Methanimine (CH_2NH) has already been observed long ago using Parkes 64 m telescope in Sgr B2 (Godfrey et al. 1973). However, the presence of λ^1 -azanylmethane is yet to be ascertained. Based on the enthalpy of formation and relative energy values shown in Table 2 methanimine appears to be the most stable candidate of CH_3N isomeric group. But enthalpy of formation is not sufficient enough to dictate the abundance of this species specifically when the system is far away from the equilibrium. It is only the reaction pathways which can dictate the final abundance of any species in the ISM. Our calculated dipole moment components (shown in Table 3) of methanimine are very close to the available experimental values. From our calculated dipole moment components, it is found that for methanimine, ‘a’ and ‘b’ type rotational transitions are the strongest whereas ‘c’ type transitions are absent.

In the case of λ^1 -azanylmethane, the strongest component of dipole moment is found to be the ‘a’ component whereas the ‘b’ component is found to be the weakest. The average dipole moment component of methanimine is found to be slightly higher than that of the λ^1 -azanylmethane. Our calculated rotational constants for methanimine are also shown in Table 4 which are found to be very close to the prevailing experimental values.

It is believed that the methanimine is primarily created within the cold ice phase. The dominated pathways are shown in the reaction range R4-R7 of Table 1. Starting with the cyanide radical, CH_2NH may form through the successive hydrogen addition reaction in ice phase. Subsequent hydrogen addition may take place in two ways: hydrogen addition with HCN could result in H_2CN (R4) or HCNH (R5). Woon (2002) pointed out that reactions R4 and R5 possess activation energy barriers of about 3647 K and 6440 K respectively. H_2CN and HCNH can further produce CH_2NH by the hydrogen addition reaction (R6 and R7 respectively). Surface network of KIDA already considered the reactions enlisted in Graninger et al. (2014) and thus HCN/HNC related chemistry is consistent. The gas phase pathways of Graninger et al. (2014) is also considered in our gas phase network. Near the higher temperatures, methanimine may be produced by the decomposition of methylamine (CH_3NH_2) (Johnson & Lovas. 1972). Recently, Suzuki et al. (2016) pointed out that this species could be produced on the interstellar ice by other reactions (R1-R3) shown in Table 1.

For the gas phase reactions G4 and G5 of Table 5, we obtain ΔG^\ddagger to be 8.37 and 10.06 Kcal/mol respectively. In Figure 2ab, chemical evolution of methanimine within the cold isothermal phase and in Figure 3 the subsequent warm-up phase is shown. Abundances are shown with respect to H_2 molecules. It is clear that during the isothermal phase, methanimine is significantly abundant in both the phases and having a peak abundance of 5.93×10^{-8} in gas phase and 3.49×10^{-6} in the ice phase. Strong decreasing slope of gas phase methanimine is observed from Figure 2a. Figure 2b also depicts a decreasing slope (during the end of the isothermal regime) of ice phase methanimine due to the production of methylamine by successive hydrogen addition reaction (R8-R9). Dashed curves in Figure 2a are shown for the gas phase abundances of all the aldimines and amines for the case where non-thermal desorption factor, a_{fac} is assumed to be 0. The gas phase abundance of methanimine with $a_{fac} = 0$ (dashed line in Figure 2a) and $a_{fac} = 0.03$ (solid line in Figure 2a) differ significantly. It is because in the isothermal phase, the gas phase contribution of methanimine is mainly coming from the ice phase via non-thermal desorption mechanism. Following KIDA database, desorption energy of methanimine is assumed to be 5534 K. It is evident that in the warm-up phase sublimation of metha-

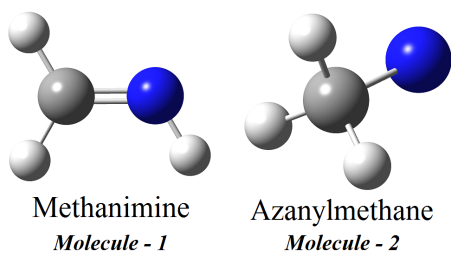


Figure 1. CH₃N isomers.

nimine occurs around 110K. In the warm-up phase (Figure 3), abundance of gas phase methanimine is significantly increased due to the efficient gas phase formation by reactions G1-G7. Peak abundance of gas phase methanimine is found to be around 1.81×10^{-09} . Our obtained values can be compared with the recent hot-core observation of methanimine $\sim 7.0 \times 10^{-08}$ in G10.47+0.03 and 3.0×10^{-9} in NGC6334F by Suzuki et al. (2016).

3.2. CH₅N Isomeric Group

Only methylamine (CH₃NH₂) belongs to this isomeric group (Figure 4) and this was already observed long ago in Sgr B2 and Ori A (Kaifu et al. 1974; Fourikis et al. 1974). In Table 2, we compare our calculated enthalpies of formation with that of the existing experimental value. We find that our calculated value with the B3LYP/6-31G(d,p) method is closer to the experimentally obtained value than that computed from the G4 composite method. Methylamine is the precursor of an amino acid (glycine) formation. Takagi & Kojima (1973); Kaifu et al. (1974) found that the c-type transitions of methylamine are 4 times stronger than the a-type transitions. We also found a very strong c-component of dipole moment shown in Table 3. Calculated total dipole moment component for methylamine is 1.2874 Debye whereas the experimentally obtained value is 1.31 ± 0.03 Debye (Table 3). Also, a very good correlation between our calculated rotational constants and experimentally obtained values can be seen from Table 4.

In the ISM, methylamine may be formed via two successive hydrogen addition reactions of methanimine in the ice phase (Godfrey et al. 1973; Suzuki et al. 2016). Woon (2002) determined that the primary step of this hydrogen addition reaction may proceed in two ways. First, hydrogenation of methanimine yields CH₃NH (R8) having activation barrier of 2134 K and second, it may produce CH₂NH₂ (R9) having activation barrier of 3170 K. Reaction R8 and R9 may also occur in the gas phase as well. From our TST calculation, we have $\Delta G^\ddagger = 7.84$ Kcal/mol for the reaction G8 of Table 5. However, we did not find a suitable transition state for the gas phase reaction G9 of Table 5. In the ice phase, R9 possesses higher activation barrier (1.485 times higher) than R8. We assume that a similar trend would be followed for the gas

phase reaction G9 and so, we assume $\Delta G^\ddagger = 11.64$ Kcal/mol for the gas phase reaction G9. Methylamine may further be produced by hydrogenation reaction of these two products by reaction numbers R10 and R11 respectively. Woon (2002) recommended that the simplest amino acid, glycine may be formed by the reaction between CH₂NH₂ and COOH radical. So, methylamine is an important product towards the formation of glycine.

Since reactions G8 and G9 possess high ΔG^\ddagger , during the isothermal phase, production of gas phase methylamine is inadequate. However, despite high activation barrier (E_a) reactions R8 and R9 would be efficiently processed on interstellar ice by quantum mechanical tunneling and populate the gas phase by the non-thermal desorption. Mainly due to the non-thermal chemical desorption phenomenon, ice phase methylamine populate the gas phase. It is clearly visible from Figure 2a that for the case of $a_{fac} = 0$, gas phase contribution of methylamine is negligible (the dashed line corresponding to the methylamine is absent in Figure 2a), So, in the isothermal phase, contribution for the gas phase methylamine is mainly comes from the ice phase. We find that in the isothermal phase, methylamine attains a peak value of 8.46×10^{-13} in the gas phase and 3.70×10^{-08} in ice phase respectively. From Figure 3, it is observed that ice phase abundance initially increases due to the increase in the mobility of the reactants. Peak ice phase abundance of methylamine is obtained to be 5.44×10^{-07} . Near the high temperature, production of gas phase methylamine significantly contributed due to (a) the enhancement of the temperature dependent rate coefficient of reactions G8 and G9 and (b) increase in the gas phase methanimine formation. The peak gas phase abundance of methylamine is found to be 5.54×10^{-07} . Our obtained values may be compared with the recent observation of methylamine (Ohishi et al. 2017). They predicted methylamine abundance $\sim 1.2 \times 10^{-08}$ in G10.47+0.03.

3.3. C₂H₅N Isomeric Group

Five isomers belong to this isomeric group (Figure 5): E-ethanimine, Z-ethanimine, ethenamine, N-methylmethanimine and aziridine. Out of these five isomers, recently, both the conformers (E and Z) of ethanimine (CH₃CHNH) had been detected in Sgr B2 (Loomis et al. 2013). From our quantum chemical calculation, we found that E-ethanimine is energetically more stable (4.35 KJ/mol by using MP2/6-311G++(d,p) and 1.2 KJ/mol by using G4 composite method) than Z-ethanimine. Quan et al. (2016) and Loomis et al. (2013) obtained an energy difference of 4.60 KJ/mol and 4.24 KJ/mol respectively between these two conformers. We have shown the enthalpy of formation values for all the species in Table 2 along with the experimentally obtained values, where available. Our calculated enthalpies of formation using B3LYP/6-31G(d,p) method are

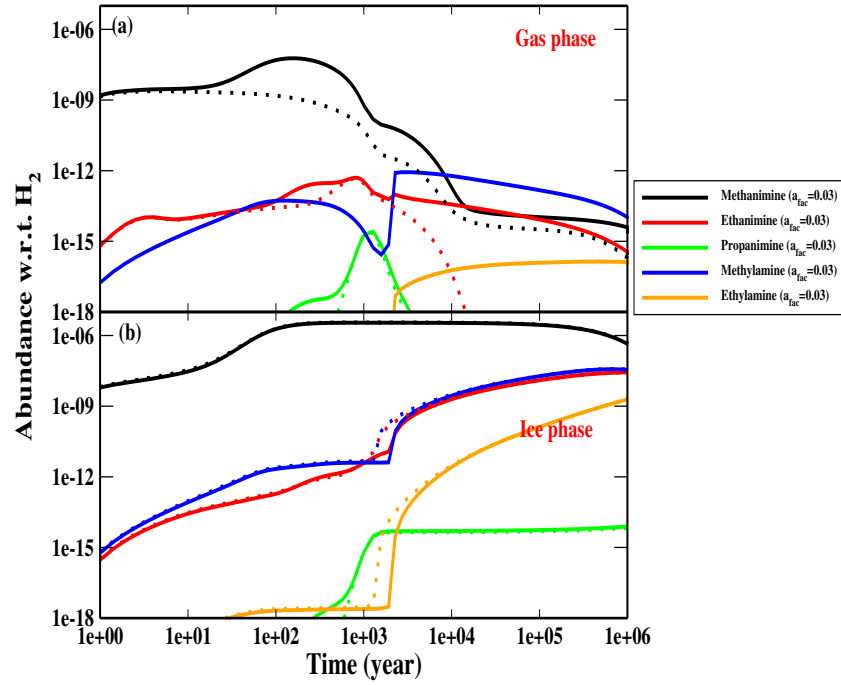


Figure 2. Chemical evolution of the aldimines and amines in the isothermal phase for $a_{fac} = 0.03$ (solid) and 0 (dashed).

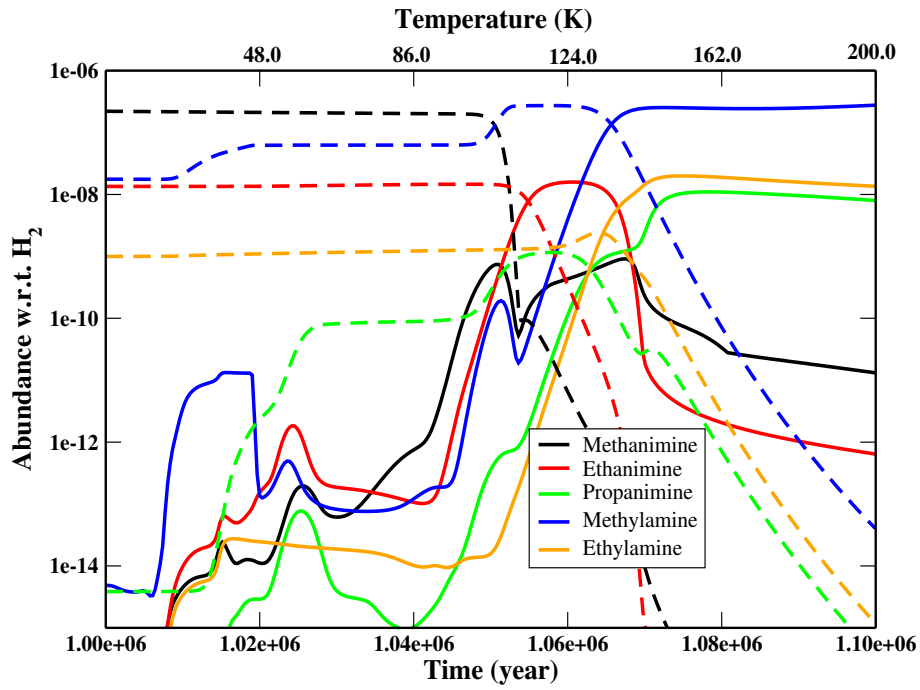


Figure 3. Chemical evolution of the aldimines and amines in the warm-up phase. Solid lines represent the gas phase species, whereas corresponding dashed lines represent the ice phase species.

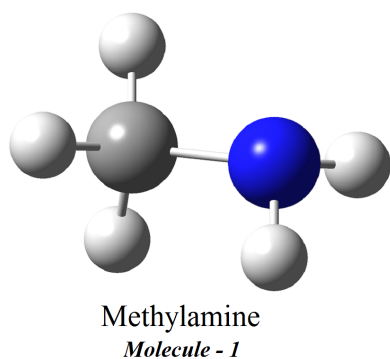


Figure 4. CH₅N isomer.

in good agreement with the experimentally obtained values of E-ethanimine, n-methylmethanimine and Aziridine. For a better assessment, in Figure 6, we show the enthalpy of formation with the molecule number noted in Table 2 and Figure 5 for C₂H₅N isomeric group. Clearly, E-ethanimine has the minimum enthalpy of formation followed by Z-ethanimine. The energy difference between these two is smaller than the other isomers of this isomeric group. Observed isomers are marked as green circles and the unobserved are marked by red circles in Figure 6.

All the dipole moment components are presented in Table 3. Our calculated values of dipole moments are compared with the existing values (Lovas et al. 1980; Lias et al. 2005). The effective dipole moment of Z-ethanimine is found to be higher than that of E-ethanimine. Charnley et al. (1995) pointed out that for an optically thin emission, an idea about the antenna temperature could be made by calculating the intensity of a given rotational transition. This intensity is proportional to $\mu^2/Q(T_{rot})$, where μ is the electric dipole moment and $Q(T_{rot})$ is the partition function at rotational temperature (T_{rot}). In Table 4, we have pointed out the rotational constants and the rotational partition function at $T_{rot} = 200$ K. In Figure 7, we have shown the plot of the expected intensity ratio (by assuming all the species of this isomeric group have same abundances) with respect to the most stable isomer (E-ethanimine) of this isomeric group (relative energy values with molecule number of all isomer of C₂H₅N isomeric group noted in Table 2). In Figure 7, the expected intensity ratios for all the species of this isomeric group are shown by considering the effective dipole moments. Since in this isomeric group, Z-ethanimine has the largest effective dipole moment, assuming the same abundances, probability of detecting Z-isomer of ethanimine will be more favourable than the other isomers of this isomeric group. From Figure 7, we can see that after E and Z isomers of ethanimine, aziridine has the strongest transition but due to its higher relative energy in comparison to E-ethanimine makes it less probable

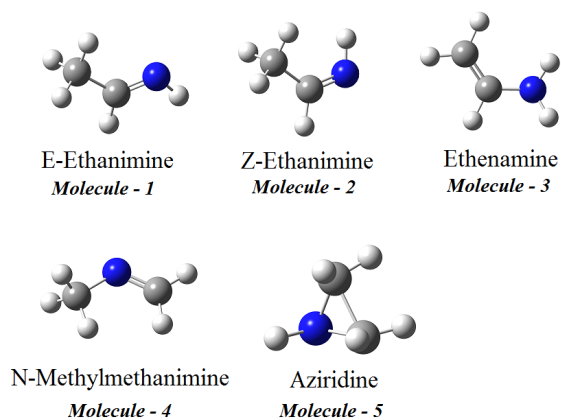


Figure 5. C₂H₅N isomers.

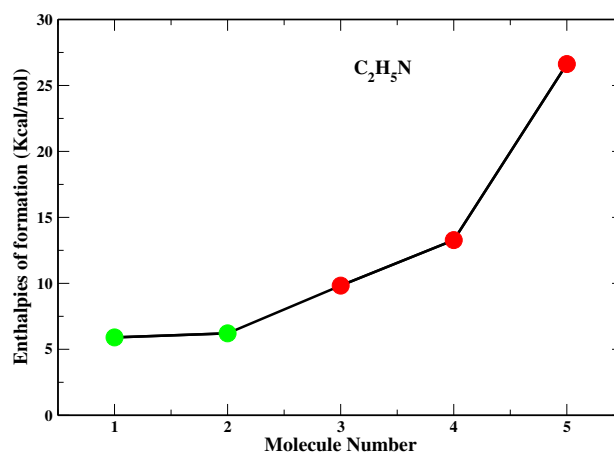


Figure 6. Enthalpy of formation of C₂H₅N isomeric group. Molecules already observed are marked as green circles and those yet to be observed are marked as red circles.

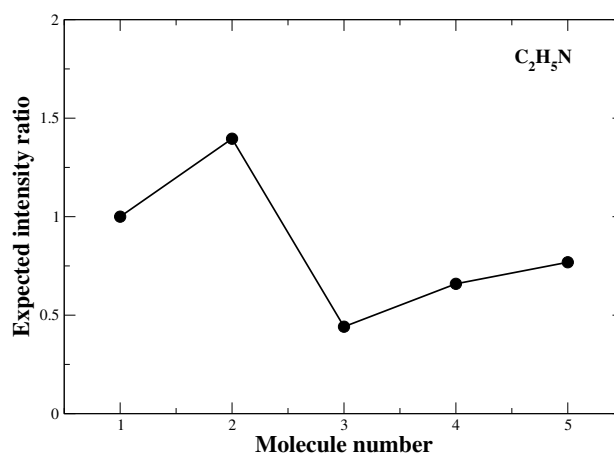


Figure 7. Expected intensity ratio of C₂H₅N isomeric group by considering the effective dipole moment of all the species.

candidate (if reaction pathways do not influence at all) for astronomical detection.

Loomis et al. (2013) mentioned that in ice phase ethanimine may be produced via two consecutive hydrogen addition reactions with CH_3CN . Quan et al. (2016) recently proposed that the first step (R14) hydrogen addition reaction with CH_3CN has the barrier of 1400 K and the second step (R15) is a radical-radical reaction and assumed to be barrier-less in nature. For the gas phase reaction of G14 of Table 5, our calculated value of ΔG^\ddagger is 10.32 Kcal/mol. Quan et al. (2016) additionally suggested that ethanimine can even be produced by the reaction between CH_3 and H_2CN in ice phase. Among the gas phase pathways, reaction between C_2H_5 and NH (reaction G23 of Table 5) may lead to CH_3CHNH . In our network, We include all the gas phase reactions mentioned in Table 5 and ice phase reactions shown in Table 1. For the gas phase barrier-less reactions, a conservative value of the rate coefficient (Vasyunin & Herbst 2013) are considered. Here, we assume only one form of ethanimine (E-ethanimine) for the purpose of our modeling.

In Figure 2ab, we have shown the chemical evolution of ethanimine in the isothermal phase and subsequently the warm-up phase is shown in Figure 3. In the isothermal phase, ethanimine has the peak value of 4.99×10^{-13} in the gas phase and 2.69×10^{-08} in the ice phase respectively. During the warm-up phase, gas phase ethanimine has a peak value of 3.17×10^{-08} . In the warm-up phase, gas phase production of ethanimine is also contributing due to the enhancement of the temperature dependent rate coefficient of reaction G14. Around 125 K, abundance of ethanimine attains a peak and started to decrease due to the efficient production of ethylamine by the successive hydrogenation reactions (R17-R18). Since the reaction R17 has a barrier, we use Eq.1 for the computation of its rate coefficient. Eq. 1 clearly says that as we are increasing the temperature, rate coefficient increases exponentially. Thus, in the warm-up phase, rate coefficient of reaction G17 increases exponentially and attain a reasonable rate ($10^{-10} \text{ cm}^3 \text{ s}^{-1}$) which means the destruction of ethanimine by the hydrogenation reaction also gradually increases and attain a quasi-steady state. At the end of our simulation (after 1.1×10^6 year), we are having an abundance of 1.27×10^{-12} for Z-ethanimine whereas the predicted abundance of Z-ethanimine $\sim 6.0 \times 10^{-11}$ by Quan et al. (2016).

3.4. $\text{C}_2\text{H}_7\text{N}$ Isomeric Group

Trans-ethylamine, gauche-ethylamine and dimethylamine belong to the $\text{C}_2\text{H}_7\text{N}$ isomeric group (Figure 8). Interestingly, no species of this isomeric group is yet to be detected in the ISM. However, the presence of ethylamine was traced in comet Wild 2 (Glavin et al. 2008). Ethylamine is the precursor of simple amino acid, glycine. It can exist in the form of two stable conformers: gauche and trans. Experiment by Hamada et al. (1986) shows that the trans conformer is slightly more stable than the gauche conformer. Our cal-

culated values are also in line with this result. We obtained that gauche conformer has 1.67 KJ/mol higher energy than its trans conformer. So, according to the enthalpy of formation and relative energies are shown in Table 2, trans-ethylamine has the least enthalpy of formation and is most stable among this isomeric group. In Figure 9, enthalpy of formation of this isomeric group is depicted with the molecule number and enthalpy of formation is noted in Table 2. In comparison with the experimentally measured enthalpies of formation, the G4 composite method overestimates the enthalpy of formation values for ethylamine and dimethylamine.

Based on the data available from our quantum chemical calculations, in Figure 10, we have shown the expected intensity ratio with respect to the species having least enthalpy of formation. Figure 10 depicts that the trans-ethylamine has the highest expected intensity ratio (~ 1) in comparison with the other two members (gauche-ethylamine has 0.97 and dimethylamine has 0.69) of this isomeric group and thus trans-ethylamine has the highest probability of its astronomical detection from this isomeric group.

Ethylamine could be formed on the grain surface via two successive hydrogen additions of ethanimine. Our calculation reveals that the first step of this hydrogenation reaction having activation barrier of 1846 K (R17). For the gas phase hydrogenation reaction (G17), our calculated ΔG^\ddagger parameter is found to be 9.98 Kcal/mol. Since the second step of this reaction is radical-radical in nature, we assume that reaction R18 may be treated as a barrier-less process. Gas and ice phase abundances of ethylamine in the isothermal phase are depicted in Figure 2ab. In the isothermal phase, we have a peak gas phase abundance of 1.19×10^{-16} and in the ice phase 1.99×10^{-09} . In the warm-up phase (Figure 3), ice phase abundance roughly remains invariant up to 125 K and then it starts to decrease sharply. Its gas phase abundance is higher and has a peak abundance of 3.98×10^{-08} .

In terms of the size of the molecule, ethanimine is more complex than methanimine. Similarly, their successors, ethylamine is more complex than methylamine. So, it may be expected that throughout the evolutionary stage, the abundances of ethanimine/ethylamine would be always less than that of methanimine/methylamine. But Figure 2ab and Figure 3 depicts that this trend is not universal for all circumstances. This is due to the fact that the formation of methanimine and its successor and ethanimine and its successor are processed through totally different channels. Their destruction rates are also different. For example, ice phase formation of methanimine mainly occurs by successive hydrogenation reactions with HCN (reaction R4 to R7) whereas ethanimine formation is mainly controlled by successive hydrogenation reactions with CH_3CN (reaction R14 and R15). Now, reactions R4 and R5 contain much higher barrier than that of the reaction R14. Since HCN is more abundant than CH_3CN , de-

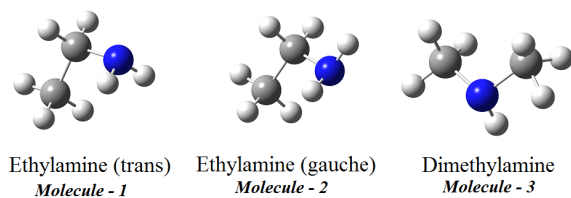


Figure 8. C_2H_7N isomers.

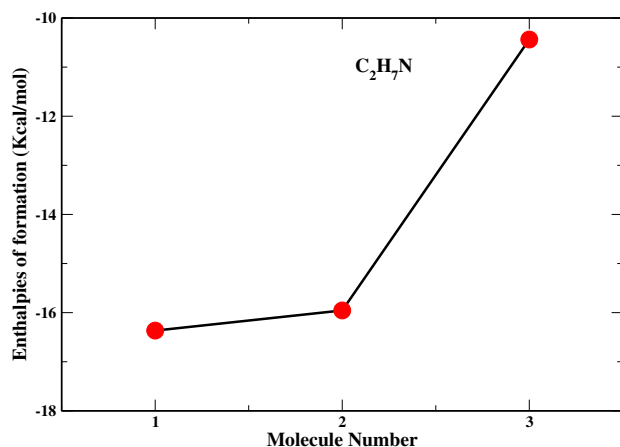


Figure 9. Enthalpy of formation C_2H_7N isomeric group.

spite high barriers involved in the formation of methanimine, in the isothermal stage, most of the time, ice phase abundance of methanimine remains higher than ethanimine. In the hot core region, due to lower activation barrier of reaction R14, ethanimine formation become more favourable. Now, methylamine is forming from methanimine (by reaction numbers R8-R10) and ethylamine is forming from ethanimine (by reaction numbers R17-R18). Once again, the activation barrier involved in case of methylamine formation (reaction R9) is higher than the barrier involved in the formation of ethylamine (reaction R17). Since, very complex chemistry is going on, abundances of these species should be compared very carefully.

Altwegg et al. (2016) showed that in 67P/Churyumov-Gerasimenko, relative abundance between methylamine and glycine is 1.0 ± 0.5 and ethylamine to glycine ratio is 0.3 ± 0.2 . Taking the maximum and minimum values from this observation, we can see that methylamine to ethylamine ratio may vary in between $\sim 1 - 15$. In order to check the correlation (if any) between the cometary ice as observed by Altwegg et al. (2016) and interstellar ice, we may focus on our ice phase evolution results of the isothermal ($T = 10$ K) phase. From our modeling results (Figure 2b), we found that in the isothermal phase (at time 10^6 year), the methylamine to ethylamine ratio to be of ~ 17.7 in the ice phase which is very close to the observed value (Altwegg et al. 2016). This suggests that

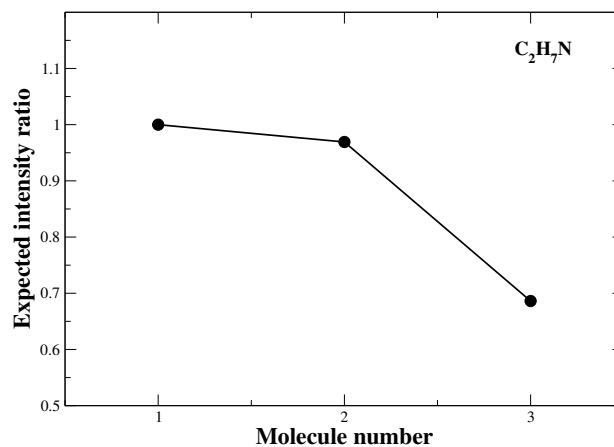


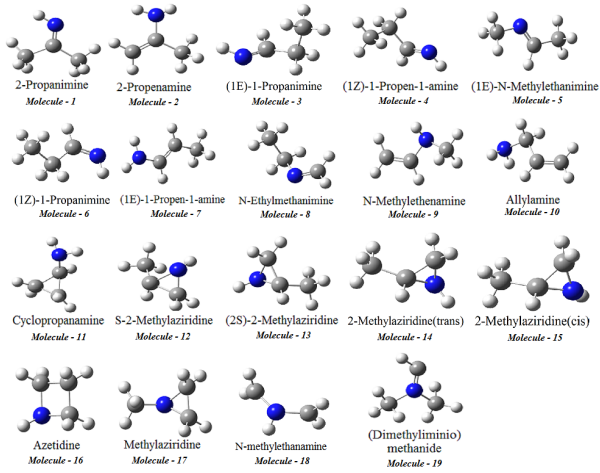
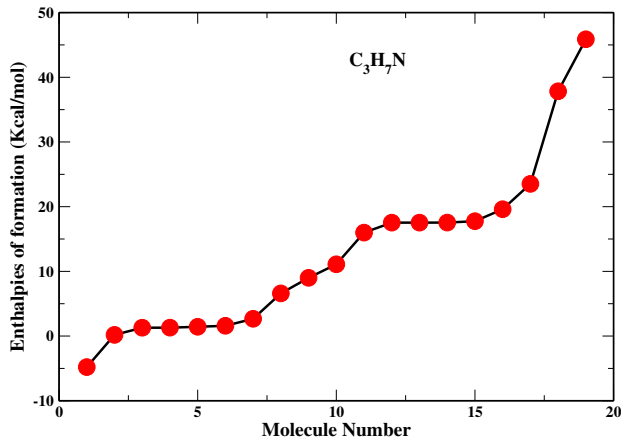
Figure 10. Expected intensity ratio of C_2H_7N isomeric group by considering the effective dipole moment of all the species.

more in depth study is required to confirm this linkage between the interstellar and cometary origin of these molecules.

3.5. C_3H_7N Isomeric Group

Nineteen isomers (Figure 11) belong to C_3H_7N isomeric group. Figure 12 depicts enthalpy of formation ($\Delta_f H^0$) of this isomeric group. In Table 2, we show the relative energies and enthalpy of formation of various isomers of this isomeric group. Only for cyclopropanamine, experimentally obtained enthalpy of formation is available and this is in close agreement with our calculated enthalpies of formation with the B3LYP/6-31G(d,p) method. Clearly, 2-propanimine is the most stable isomer of this group followed by 2-propenamine. Next species in this sequence is (1E)-1-propanimine. (1E)-1-propanimine has the lower energy than that of the (1Z)-1-propanimine.

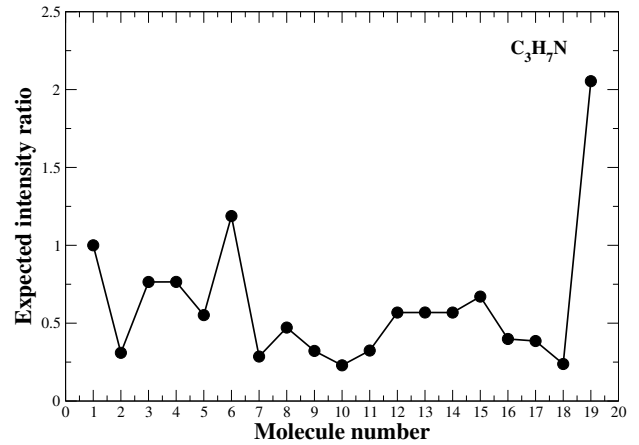
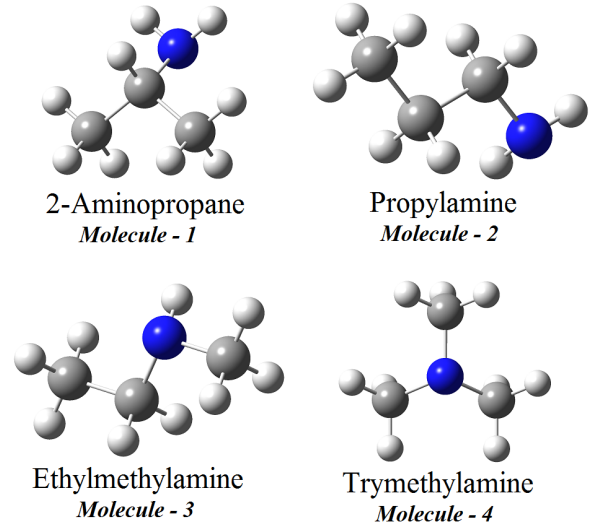
Though (Dimethyliminio)methanide (molecule no. 19) has the highest enthalpy of formation and is the least stable of the species in this isomeric group, interestingly, our calculation listed in Table 4 shows that it possesses the highest effective electric dipole moment. (1Z)-1-propanimine (molecule no. 6) is found to be having the second highest effective dipole moment in this isomeric group. However, it is found that the a-type transitions of 1-Z propanimine are the strongest among all the species of C_3H_7N isomeric group. Figure 13, shows the expected intensity ratio (by considering the effective dipole moment) with respect to the most stable (as well as the species having least enthalpy of formation) isomer. From Figure 13, it is clear that if the abundances of all these isomeric species are assumed to be the same, then (Dimethyliminio)methanide and (1Z)-1-propanimine may be the most probable candidate for the astronomical detection from this group. Since (Dimethyliminio)methanide is not very stable species, it does not have high probability of detection. Thus, based on the stability, enthalpy of formation and expected intensity ratio, (1Z)-1-propanimine is the most suit-

Figure 11. C_3H_7N isomers.Figure 12. Enthalpy of formation of C_3H_7N isomeric group.

able species for the future astronomical detection from this isomeric group. However, it is the reaction pathways which can ultimately decide the fate of this species.

Methanimine and ethanimine have already been observed in the ISM and (1Z)1-propanimine may be the next probable candidate for astronomical detection. To the best of our knowledge, the astronomical searches of (1Z)-1-propanimine are yet to be reported in the literature. So (1Z)-1-propanimine remains the best candidate for astronomical observation among all the isomers of C_3H_7N isomeric group.

(1Z)-1-propanimine may be formed via two sequential H addition reaction on ice with propionitrile (CH_3CH_2CN), where propionitrile may be produced by the radical-radical barrier-less interaction between C_2H_5 and CN. Instead of radical reactant CN, H_2CN may also react with C_2H_5 to form propanimine directly by the reaction R19. This reaction is assumed to be barrier-less in nature. We found that the first step (R21) of hydrogen addition with propionitrile has a barrier of 2712 K and the second step (R22) is a radical-radical inter-

Figure 13. Expected intensity ratio of C_3H_7N isomeric group by considering the effective dipole moment of all the species.Figure 14. C_3H_9N isomers.

action. We assume that the second step of this sequence is barrier-less. For the gas phase hydrogenation reaction (G21), our calculated ΔG^\ddagger parameter is found to be 11.03 Kcal/mol. In Figure 2ab and Figure 3, we have shown the time evolution of propanimine (1Z)-1-propanimine). It is evident from the figure that the production of (1Z)-1-propanimine is only favourable in the hot core region. We have a peak gas phase abundance of (1Z)-1-propanimine (propanimine) 2.20×10^{-08} .

3.6. C_3H_9N Isomeric Group

We consider 4 species (Figure 14) from this isomeric group namely, 2-aminopropane, propylamine, ethylmethanimine and trimethylamine. Methanimine is the most stable isomer of the CH_5N group and ethylamine is the most stable isomer of the C_2H_7N isomeric group. In general,

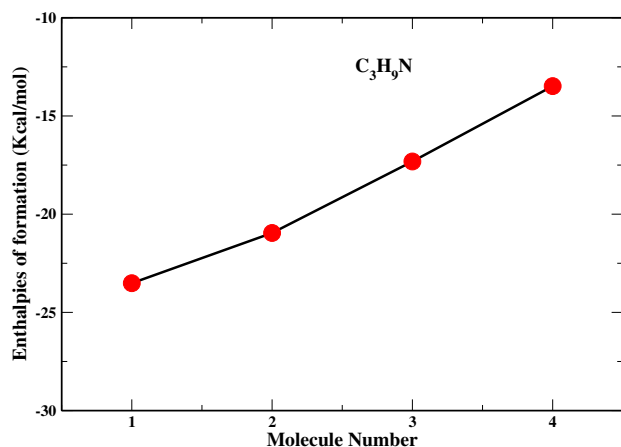


Figure 15. Enthalpy of formation of C₃H₉N isomeric group.

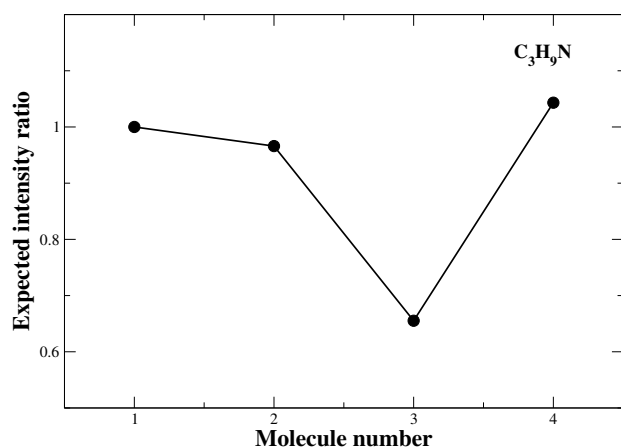


Figure 16. Expected intensity ratio of C₃H₉N isomeric group by considering the effective dipole moment of all the species.

it is expected that the branched chain molecules would be comparatively more stable than the other species of an isomeric group. Recently, *Etim et al. (2017)* showed that Isopropyl cyanide, a branched chain molecule is the most stable within C₄H₇N isomeric group and Tert-butyl cyanide, another branched chain molecule is the most stable species within C₅H₉N isomeric group. Following the similar trend, we found that 2-aminopropane, a branched chain molecule of C₃H₉N isomeric group is the most stable isomer of this group. 2-aminopropane is found to be 2.51 Kcal/mol more stable than the propylamine. In Figure 15, we have shown the enthalpy of formation of these four species. Relative energy and enthalpy of formation of these four isomers are shown in Table 2 and arranged based on their enthalpy of formation. Theoretically calculated and experimentally obtained enthalpies of formation values have a similar trend. From Table 2, it is evident that the calculated enthalpies of formation with the B3LYP/6-31G(d,p) method appears to be comparatively closer to the experimental values than that of the G4 composite method. Expected intensity ratio with respect

to the species having the minimum enthalpy of formation is shown in Figure 16. Interestingly, though trimethylamine which has the lowest total dipole moment value among this isomeric group, the rotational intensity is found to be maximum because of its lower partition function. More interestingly, due to its unique structure, rotational constants A and B have the same value (8.75934 GHz). We also have reconfirmed this unique nature of trimethylamine (an oblate symmetric top species) by using the G4 composite method and HF/6-31G(3df) method. Since the production of propanimine from the very last isomeric group of this sequence, C₃H₇N, is not significantly higher, we have not prepared any reaction pathways for the formation of any species from the C₃H₉N isomeric group.

In this section, we have investigated about the chemical abundances of some specific groups of amine and aldimines. Results presented here, clearly shows that imines (methanimine, ethanimine and propanimine) and amines (methylamine and ethylamine) may be efficiently produced in the ice phase (either in the isothermal or in the hot core regime). Depending upon the barrier energy considered, Figure 3 depicts a nice trend of sublimation. For example, we have adopted binding energy of ethylamine and methylamine to be 6480 K and 6584 K respectively. Maintaining the trend, ethylamine starts to sublime faster than methylamine. Similarly, maintaining the trend of binding energies (5534 K, 5580 K and 6337 K for methanimine, ethanimine and propanimine respectively) sublimation sequence is also obtained for the imines as well.

4. ASTROPHYSICAL IMPLICATIONS OF THIS WORK

Methanimine is an important prebiotic molecule which is believed to be the precursor molecule for the formation of simplest amino acid, glycine. It was mentioned earlier that this species is detected in the ISM. Most interestingly, this species is also detected in the upper atmosphere of Titan (the massive moon of Saturn) (*Vuitton et al. 2006*). Present atmosphere of Titan resembles the primeval atmosphere of Earth and thus thought to be important for the abiotic synthesis. Our present study found that methanimine may be further processed to form methylamine which is yet to be observed in the Titan's atmosphere. Modeling the Titan's atmosphere is out of scope for this paper. However, the inclusion of proposed pathways in the modeling of Titan atmosphere may come up with the higher mixing ratios of higher order imines and amines in Titan's atmosphere.

We have performed radiative transfer modeling (both with LTE and non-LTE consideration) which may be useful for the future astronomical observation of ethylamine and propanimine in the ISM. For the calculation of the line parameters by using LTE approximation, we use CASSIS interactive spectrum analyzer (<http://cassis.irap.omp.eu/>). In Table

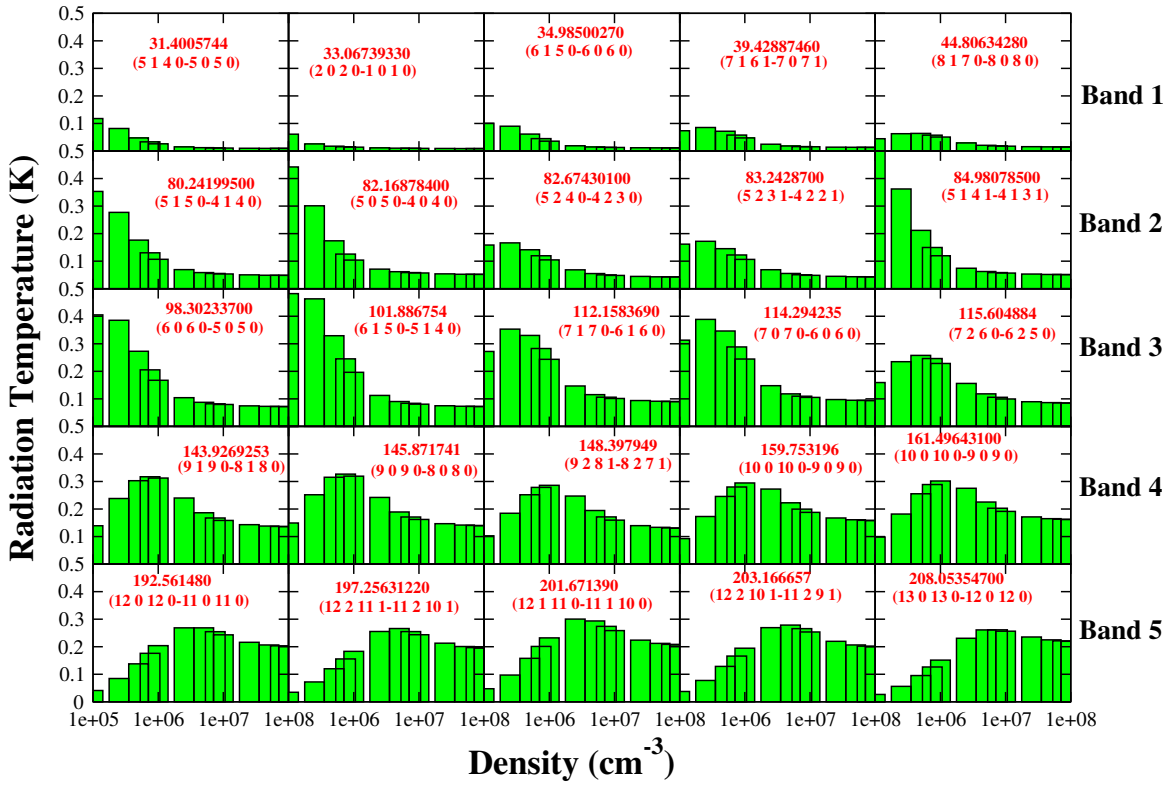


Figure 17. Density variation of the intensity of various transitions of ethylamine by considering non-LTE approximation.

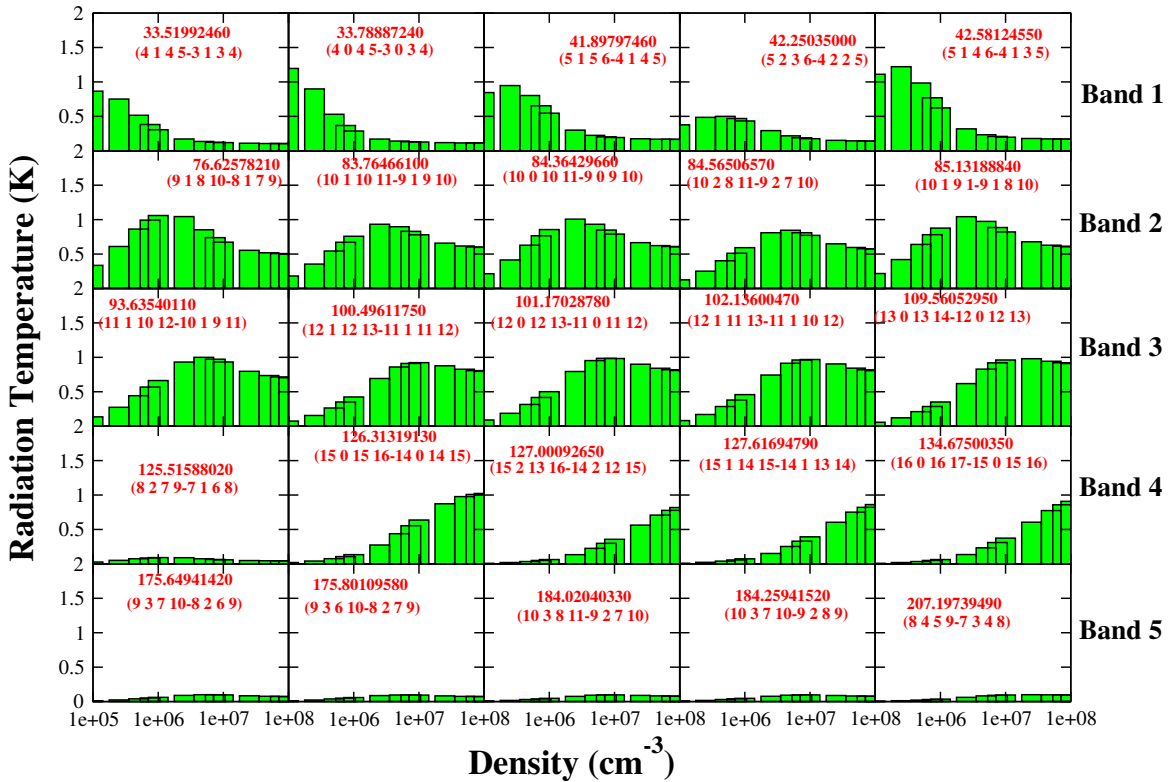


Figure 18. Density variation of the intensity of various transitions of propanimine by considering non-LTE approximation.

6, we have pointed out some of the most intense transitions of ethylamine that fall in ALMA Bands 1-5. Required spectroscopic details for ethylamine is available in <https://www.astro.uni-koeln.de/cdms/catalog> Similarly, in Table 7, intense transitions of propanimine is shown. Required spectroscopic details for (1Z)-1-propanimine is obtained by including the experimentally obtained rotational and distortional constants in SPCAT program (Pickett 1991). For preparing these tables, we have used column density of $H_2 = 10^{23} \text{ cm}^{-2}$, $n_H = 10^7 \text{ cm}^{-3}$, excitation temperature = 130 K, FWHM= 10 km/s, $V_{LSR} = 64 \text{ km/s}$, source size = $3''$, Abundance of ethylamine = 4.0×10^{-08} and abundance of propanimine to be 2×10^{-8} .

We have also performed non-LTE calculation by using RADEX programme (Van der Tak et al. 2007). Collisional data file for ethylamine and propanimine is yet to be available in any database. Thus, we prepare the collisional data file in the appropriate format from the spectral information available in JPL (for trans-ethylamine) and from our calculation (for (1Z)-1-propanimine). Altogether we have considered transitions between 251 energy levels. Here, we assume H_2 as the colliding partner. In order to estimate the line profile with non-LTE, here, we have estimated the collisional rate of ethylamine and propanimine by following the relation mentioned in Sharma & Chandra (2001). Sharma & Chandra (2001) estimated the collisional rate coefficient for a downward transition of an asymmetric top molecule, cyclopropene at temperature ‘T’ by,

$$C(J'' K''_a K''_c \rightarrow J' K'_a K'_c) = [1 \times 10^{-11} / (2J'' + 1)] \sqrt{T/30}. \quad (3)$$

In Table 8 and Table 9, we have pointed out most intense transitions of trans-ethylamine and (1Z)-1-propanimine respectively which are falling within the ALMA band 1-5. For the non-LTE calculations, we have used column density of ethylamine to be 10^{15} cm^{-2} and column density of propanimine to be $5.0 \times 10^{14} \text{ cm}^{-2}$, $n_H = 10^7 \text{ cm}^{-3}$, excitation temperature = 130 K, FWHM= 10 km/s.

For the transitions pointed out in Table 8 and Table 9, we have studied the density variation of ethylamine (Figure 17)

and propanimine (Figure 18) with the non-LTE consideration. Figures 17 and 18 would be served as a very useful starting point for the observation of ethylamine and propanimine in the ISM. It is to be noted that in absence of the measured or calculated collisional data file, we have used our estimated collisional rate but it is known that the non-LTE transitions are heavily dependent upon collisional rates and consideration of random rates may end up with some misleading results.

5. CONCLUSIONS

In this work, we examine the possibility of detecting various molecules that belong to six specific isomeric groups. We have used the chemical abundance, enthalpy of formation, optimized energy, and expected intensity ratio to shortlist some species that might be the viable candidates for future astronomical detection in the ISM. According to our calculation, ethylamine remains the most suitable candidate for future astronomical detection in the ISM. (1Z)-1-propanimine also may be a potential candidate. From our gas-grain chemical modeling, we see that the precursor molecules (methylamine and ethylamine) of glycine could efficiently be formed around the star-forming region. Moreover, radiative transfer modeling (LTE and non-LTE) has been employed for the detection of these species in the ISM.

ACKNOWLEDGMENTS

M.S. gratefully acknowledges DST, the Government of India for providing financial assistance through DST-INSPIRE Fellowship [IF160109] scheme. A.D. acknowledges the ISRO respond (grant no. ISRO/RES/2/402/16-17) and DST project (Grant No. SB/S2/HEP-021/2013) for financial support. B.B. acknowledges DST-INSPIRE Fellowship [IF170046] for providing partial financial assistance.

Software: Gaussian 09 (Frisch et al. 2013), SPCAT (Pickett 1991), CASSIS (<http://cassis.cesr.fr>), RADEX (Van der Tak et al. 2007)

REFERENCES

- Altwegg, K., Balsiger, H., Bar-Nun, A., et al. 2016, *SciA*, 2, e1600285
- Bak, B., & Skaarup, S. 1971, *JMoSt*, 10, 385
- Brown, R. D., Godfrey, P. D., & Winkler, D. A. 1980, *AJCh*, 33, 1
- Chakrabarti, S., & Chakrabarti, S. K. 2000a, *A&A*, 354, L6
- Chakrabarti, S. K., & Chakrabarti, S. 2000b, *InJPh*, 74B, 97
- Chakrabarti, S. K., Das, A., Acharyya, K., & Chakrabarti, S. 2006a, *A&A*, 457, 167
- Chakrabarti, S. K., Das, A., Acharyya, K., & Chakrabarti, S. 2006b, *BASI*, 34, 299
- Chakrabarti, S. K., Majumdar, L., Das, A., & Chakrabarti, S. 2015, *Ap&SS*, 357, 90
- Charnley, S. B., Kress, M. E., Tielens, A. G. G. M., & Millar, T. J. 1995, *ApJ*, 448, 232
- Cronin, J. R., & Chang, S. 1993, *The Chemistry of Life's Origins*, ed. J. Greenberg, M., Mendoza-Gomez, C. X., Pirronello, V. (Dordrecht: Kluwer), 416, 209

- Curtiss, L. A., Raghavachari, K., Redfern, P. C., & Pople, J. A. 1997, *JChPh*, 106, 1063
- Curtiss, L. A., Redfern, P. C., & Raghavachari, K. 2007a, *JChPh*, 126, 084108
- Das, A., Chakrabarti, S. K., Acharyya K., & Chakrabarti, S. 2008a, *NewA*, 13, 457
- Das, A., Acharyya, K., Chakrabarti, S. & Chakrabarti, S. K., 2008b, *A&A*, 486, 209
- Das, A., Acharyya, K. & Chakrabarti, S. K., 2010, *MNRAS* 409, 789
- Das, A., & Chakrabarti, S. K. 2011, *MNRAS*, 418, 545
- Das, A., Majumdar, L., Chakrabarti, S. K., & Chakrabarti, S. 2013a, *NewA*, 23, 118
- Das, A., Majumdar, L., Chakrabarti, S. K., Saha, R., & Chakrabarti, S. 2013b, *MNRAS*, 433, 3152
- Das, A., Majumdar, L., Chakrabarti, S. K., & Sahu, D. 2015a, *NewA*, 35, 53
- Das, A., Majumdar, L., Sahu, D., Gorai, P., Sivaraman, B., & Chakrabarti, S. K. 2015b, *ApJ*, 808, 21
- Das, A., Sahu, D., Majumdar, L., & Chakrabarti, S. K. 2016, *MNRAS*, 455, 540
- Elsila, J. E., Dworkin, J. P., Bernstein, M. P., Martin, M.P., & Sandford, S. A. 2007, *ApJ*, 660, 911
- Etim, E., Gorai, P., Das, A., Chakrabarti, S. K. & Arunan, E. 2016, *ApJ*, 832, 144
- Etim, E., Gorai, P., Das, A. & Arunan, E. 2017, *EPJD*, 71, 86
- Eyring, H. 1935, *JChPh*, 3, 107
- Fischer, E., & Botskor, I. 1982, *JMoSp*, 91, 116
- Fischer, E., & Botskor, I. 1984, *JMoSp*, 104, 226
- Fortman, S. M., Neese, C. F., & De Lucia, F. C. 2014, *ApJ*, 782, 75
- Fourikis, N., Takagi, K., & Morimoto, M. 1974, *ApJL*, 191, L139
- Frenkel, M., Marsh, K. N., Wilhoit, R. C., et al. 1994, *Thermodynamics of Organic Compounds in the Gas State*, Thermodynamics Research Center, Vol. 1, CRC Press.
- Frisch, M. J., Trucks, G. W., Schlegel, H. B., et al. 2013, *Gaussian 09*, Revision D.01, Gaussian, Inc., Wallingford CT.
- Garrod, R. T., & Herbst, E. 2006, *A&A*, 457, 927
- Garrod, R. T., Wakelam, V., & Herbst, E. 2007, *A&A*, 467, 1103
- Garrod, R. T. 2013, *ApJ*, 765, 60
- Glavin, D. P., Dworkin, J. P., & Sandford, S. A. 2008, *M&PS*, 43(1–2), 399
- Godfrey, P. D., Brown, R. D., Robinson, B. J., & Sinclair, M. W. 1973, *ApJ*, 13, L119
- Gorai, P., Das, A., Das, A., Sivaraman, B., Etim, E. E., & Chakrabarti, S. K. 2017a, *ApJ*, 836, 70
- Gorai, P., Das, A., Majumdar, L., Chakrabarti, S. K., Sivaraman, B., & Herbst, E. 2017b, *MolAs*, 6, 36
- Graninger, D.M., Herbst, E., Öberg, K.I., & Vasyunin, A.I. 2014, *ApJ*, 787(1), 74
- Hamada, Y., Tsuboi, M., Yamanouchi, K., & Kuchitsu, K. 1986, *JMoSt*, 146, 253
- Hasegawa, T., Herbst, E., & Leung, C.M. 1992, *ApJ*, 82, 167
- Hendricksen, D., & Harmony, M. 1969, *JChPh*, 51, 700
- Herbst, E. 2006, in *Springer Handbook of Atomic, Mol. & Opt. Phys.*, ed. G.W.F. Drake (New York: Springer), 561
- Herzberg, G., *Molecular spectra and molecular structure*. Vol. 3: *Electronic spectra and electronic structure of polyatomic molecules*, New York: Van Nostrand, Reinhold, 1966.
- Holtom, P. D., Bennett, C. J., Osamura, Y., Mason, N. J., & Kaiser, R. I. 2005, *ApJ*, 626, 940
- Johnson, D. R., & Lovas, F. J. 1972, *CPL*, 15, 65
- Kaifu, N., Morimoto, M., Nagane, K., Akabane, K., Iguchi, T., & Takagi, K. 1974, *ApJL*, 191, L135
- Lakard, B. 2003, *Int. Elec. Conf. Mol. Des.*, Bochem press, <http://www.biochempress.com>.
- Landolt, H., Börnstein, R., & Hellwege, K. H. 1974, *Molecular Constants from Microwave, Molecular Beam, and Electron Spin Resonance Spectroscopy*, Vol. 6, Springer.
- Leung, C. M., Herbst, E., & Huebner, W. F. 1984, *ApJS*, 56, 231
- Lias, S., Linstrom, P. J., Mallard, W. G. (Eds.), *NIST Chemistry WebBook*, NIST Standard Reference Database Number 69, <http://webbook.nist.gov>, Gaithersburg MD, 2005.
- Loomis, R. A., Zaleski, D. P., Steber, A. L., et al. 2013, *ApJL*, 765, L9
- Lovas, F. J., Suenram, R. D., Johnson, D. R., Clark, F. O., & Tiemann, E. 1980, *JChPh*, 72, 4964
- Majumdar, L., Das, A., Chakrabarti, S. K., & Chakrabarti, S. 2012, *RAA*, 12, 1613
- Majumdar, L., Das, A., Chakrabarti, S. K., & Chakrabarti, S. 2013, *NewA*, 20, 15
- Majumdar, L., Das, A., & Chakrabarti, S. K. 2014a, *A&A*, 562, A56
- Majumdar, L., Das, A., & Chakrabarti, S. K. 2014b, *ApJ*, 782, 73
- Margulès, L., Motiyenko, R. A., Guillemin, J. C., & Cernicharo, J., 70th International Symposium on Molecular Spectroscopy: June 22-26, 2015 at The University of Illinois at Urbana-Champaign. Talk RI07, International Symposium on Molecular Spectroscopy (CHAMPAIGN-URBANA, ILLINOIS)
- McElroy, D., Walsh, C., Marckwick, A. J., Cordiner, M. A., Smith, K., Millar, T. J. 2013, *A&A*, 550, 36
- McMillan, J. P., Fortman, S. M., Neese, C. F., & De Lucia, F. C. 2014, *ApJ*, 795, 56
- Mehrotra, S. C., Griffin, L. L., Britt, C. O., & Boggs, J.E. 1977, *JMoSp*, 64, 244
- Müller, H. S. P., Belloche, A., Xu, L., et al. 2016, *A&A*, 587, A92
- Nelson Jr, R. D., Lide Jr, D. R., & Maryott, A. A. 1967, *Selected Values of electric dipole moments for molecules in the gas phase*, (No. NSRDS-NBS10). National Standard Reference Data System.

- Ohishi, M., Suzuki, T., Hirota, T., Saito, M. & Kaifu, N. 2017, arXiv:1708.06871
- Osmont, A., Catoire, L., Gökalp, I., & Yang, V. 2007, CoFl, 151, 262
- Pearson Jr, R., & Lovas, F.J. 1977, JChPh, 66(9), 4149
- Pickett, H. M. 1991, JMoSp, 148, 371
- Quan, D., Herbst, E., Osamura, Y., & Roueff, E. 2010, ApJ, 725, 2101
- Quan, D., Herbst, E., Corby, J. F., Durr, A., & Hassel, G. 2016, ApJ, 824, 129
- Ruaud, M., Wakelam, V., Hersant, F. 2016, MNRAS, 459, 3756
- Sahu, D., Das, A., Majumdar, L., & Chakrabarti, S. K. 2015, NewA, 38, 23
- Sastry, K. V. L. N., & Curl Jr, R. F. 1964, JChPh, 41(1), 77
- Sil, M., Gorai, P., Das, A., Sahu, D., & Chakrabarti, S. K. 2017, EPJD, 71(2), 45
- Sharma, A. K., & Chandra, S. 2001, A&A, 376, 333
- Suzuki, T., Ohishi, M., Hirota, T., Saito, M., Majumdar, L., & Wakelam, V. 2016, ApJ, 825, 1
- Takagi, K., & Kojima, T. 1973, ApJL, 181, L91
- Theule, P., Borget, F., Mispelaer, F., et al. 2011, A&A, 534, A64
- Van der Tak, F. F. S., Black, J. H., Schöier, F. L., Jansen, D. J., van Dishoeck, E. F. 2007, A&A 468, 627
- Vasyunin, A. I., & Herbst, E. 2013, ApJ, 769, 34
- Vuitton, V., Yelle, R. V., Anicich, V. G. 2006, ApJ, 647, 175
- Wollrab, J. E., & Laurie, V. W. 1968, JChPh, 48(1), 5058
- Woon, D. E. 2002, ApJL, 571, L177

Table 2. Enthalpy of Formation and Electronic Energy (E0) with Zero Point Energy (ZPE) and Relative Energy (in bracket) with G4 Composite Method for All Species of Six Isomeric Groups.

Number	Species	Astronomical Status	E0+ZPE	Calculated $\Delta_f H^0$	Experimental $\Delta_f H^0$
			in Hartree/particle	using G4 composite method	(in Kcal/mol)
			(Relative Energy	(using B3LYP/6-31G(d,p) method)	
			in Kcal/mol)	(in Kcal/mol)	
CH₃N Isomeric Group					
1.	Methanimine	observed ^b	-94.596377 (0.00)	18.2604366 (20.0748878)	—
2.	λ^1 -Azanylmethane	not observed	-94.519754 (48.08)	66.3715977 (66.9874996)	—
CH₅N Isomeric Group					
1.	Methylamine	observed ^{c,d}	-95.802182 (0.00)	-9.00194363 (-7.3082602)	-5.37763 ^a
C₂H₅N Isomeric Group					
1.	E-Ethanamine	observed ^e	-133.896198 (0.00)	5.90189865 (7.9892830)	5.74 ^f
2.	Z-Ethanamine	observed ^e	-133.895732 (0.29)	6.20797719 (8.3293932)	—
3.	Ethenamine	not observed	-133.889919 (3.94)	9.8284533 (12.7953785)	—
4.	N-Methylmethanimine	not observed	-133.884403 (7.40)	13.275162 (15.5507728)	10.51625 ^f
5.	Aziridine	not observed	-133.862508 (21.14)	26.62315 (29.3566098)	30.11472 ^a
C₂H₇N Isomeric Group					
1.	Ethylamine (trans)	not observed	-135.094044 (0.00)	-16.366079 (-14.5306661)	—
2.	Ethylamine (gauche)	not observed	-135.09341 (0.40)	-15.955933 (-14.1008221)	-11.3528 ^a
3.	Dimethylamine	not observed	-135.084612 (5.92)	-10.437412 (-8.4344111)	-4.445507 ^a
C₃H₇N Isomeric Group					
1.	2-Propanimine	not observed	-173.193699 (0.00)	-4.7991787 (-2.2671314)	—
2.	2-Propenamine	not observed	-173.18563 (5.06)	0.18444024 (3.5818848)	—
3.	(1E)-1-Propanimine	not observed	-173.183877 (6.163)	1.287921 (3.7186819)	—
4.	(1Z)-1-Propen-1-amine	not observed	-173.183875 (6.164)	1.2981179 (3.7205644)	—
5.	(1E)-N-Methylethanamine	not observed	-173.183821 (6.20)	1.4335242 (4.0067087)	—
6.	(1Z)-1-Propanimine	not observed	-173.183423 (6.45)	1.59211071 (4.0393392)	—
7.	(1E)-1-Propen-1-amine	not observed	-173.181835 (7.44)	2.6644726 (5.9243778)	—
8.	N-Ethylmethanimine	not observed	-173.17536 (11.51)	6.5932994 (12.4893824)	—
9.	N-Methylethanamine	not observed	-173.171735 (13.78)	9.0000089 (12.4893824)	—
10.	Allylamine	not observed	-173.168277 (15.95)	11.096984 (14.2338589)	—
11.	Cyclopropanamine	not observed	-173.159802 (21.27)	15.985053 (18.7632226)	18.475 ^a
12.	S-2-Methylaziridine	not observed	-173.157389 (22.7846)	17.531164 (20.4380455)	—
13.	(2S)-2-Methylaziridine	not observed	-173.157388 (22.7853)	17.535559 (20.4405556)	—
14.	2-Methylaziridine (trans)	not observed	-173.157386 (22.7865)	17.543877 (20.4393006)	—
15.	2-Methylaziridine (cis)	not observed	-173.156991 (23.03)	17.7562713 (20.7574479)	—
16.	Azetidine	not observed	-173.1536 (25.16)	19.607872 (22.3205741)	—
17.	Methylaziridine	not observed	-173.147784 (28.81)	23.520139 (26.5719511)	—
18.	N-Methylethanamine	not observed	-173.126259 (42.32)	37.837958 (41.5192279)	—
19.	(Dimethyliminio)methanide	not observed	-173.112784 (50.77)	45.881231 (50.7837785)	—
C₃H₉N Isomeric Group					
1.	2-Aminopropane	not observed	-174.385779 (0.00)	-23.5149351 (-21.4656727)	-20.0048 ^a
2.	Propylamine	not observed	-174.381773 (2.51)	-20.9566988 (-18.7880896)	-16.7543 ^a
3.	Ethylmethylamine	not observed	-174.375953 (6.16)	-17.3159833 (-15.0857834)	—
4.	Trimethylamine	not observed	-174.369667 (10.11)	-13.4808824 (-10.9573983)	-5.64054 ^a

NOTE— Additional computation of enthalpy of formation by the B3LYP/6-31G(d,p) level of theory is pointed out in parentheses.

^a Frenkel et al. (1994), ^b Godfrey et al. (1973), ^c Kaifu et al. (1974), ^d Fourikis et al. (1974), ^e Loomis et al. (2013),

^f NIST Chemistry Webbook (<http://webbook.nist.gov/chemistry>)

Table 3. Calculated Dipole Moment Components for All Species of Six Isomeric Groups with HF/6-31G(3df) Method.

Number	Species	μ_a (in Debye)	μ_b (in Debye)	μ_c (in Debye)	μ_{tot} (in Debye)
CH₃N Isomeric Group					
1.	Methanimine	-1.5115 [-1.4708] (-1.300 ^g)	-1.4556 [-1.4968] (-1.500 ^g)	0.0000 [0.0000] (0.000 ^g)	2.0985 (2.000 ^g)
2.	λ^1 -Azanylmethane	-1.9499 [-1.9556]	-0.0176 [-0.0000]	0.1483 [-0.0000]	1.9556
CH₅N Isomeric Group					
1.	Methylamine	0.4410 [-0.2516]	0.2771 [0.0000]	1.1774 [-1.2626]	1.2874 (1.310 ^h)
C₂H₅N Isomeric Group					
1.	(E)-Ethanamine	0.2063 [-0.8836]	-2.0884 [-1.9256]	0.2912 [-0.0000]	2.1187 (1.900 ^h)
2.	(Z)-Ethanamine	0.6062 [2.5103]	-2.3957 [-0.3950]	0.5926 [0.0020]	2.5412
3.	Ethenamine	0.5514 [0.9302]	1.0539 [0.0309]	-0.7109 [-1.0266]	1.3857
4.	N-Methylmethanimine	-0.2812 [-0.1599]	1.0514 [-1.6496]	1.2499 [-0.0000]	1.6573 (1.530 ⁱ)
5.	Aziridine	1.6649 [0.0007]	-0.2522 [-0.9880]	0.1768 [-1.3749]	1.6931 (1.90±0.01 ^h)
C₂H₇N Isomeric Group					
1.	Ethylamine (trans)	0.8802 [0.9708]	-0.1949 [0.8132]	0.8894 [-0.0000]	1.2664 (1.304±0.011 ^h)
2.	Ethylamine (gauche)	-0.5839 [0.1620]	-1.0489 [-0.6498]	-0.2731 [-1.0335]	1.2315 (1.220 ^h)
3.	Dimethylamine	0.1499 [-0.0000]	-0.9771 [-0.2641]	-0.1444 [0.9635]	0.9991 (1.030 ^h)
C₃H₇N Isomeric Group					
1.	2-Propanimine	1.1894 [1.3134]	-1.9000 [-2.0677]	0.9879 [-0.0005]	2.4496
2.	2-Propenamine	0.4017 [-0.1912]	0.4670 [0.9101]	-1.1975 [-0.9739]	1.3467
3.	(1E)-1-Propanimine	-1.0918 [1.0653]	-1.5598 [-0.7588]	0.8831 [1.6414]	2.0987
4.	(1Z)-1-Propen-1-amine	-0.1209 [-1.0650]	1.0920 [-0.7572]	1.7882 [-1.6423]	2.0987
5.	(1E)-N-Methylethanamine	-1.3457 [0.4136]	-0.2385 [-1.5828]	0.8994 [0.0000]	1.6360
6.	(1Z)-1-Propanimine	-2.1065 [2.4499]	1.5775 [0.9613]	-0.0300 [-0.0188]	2.6318
7.	(1E)-1-Propen-1-amine	1.0898 [-0.6029]	-0.4583 [-0.0139]	-0.2748 [1.0534]	1.2138
8.	N-Ethylmethanimine	-1.4418 [0.2444]	-0.6595 [-0.8449]	-0.0489 [-1.3201]	1.5862
9.	N-Methylethanamine	-1.2679 [1.0808]	-0.0583 [0.0768]	-0.0886 [0.6669]	1.2723
10.	Allylamine	-0.1645 [-0.7685]	-1.1175 [-0.8256]	-0.2388 [-0.2466]	1.1545 (\approx 1.2 ^h)
11.	Cyclopropanamine	0.0564 [-0.4994]	0.9405 [0.0003]	-0.8402 [1.1307]	1.2361 (1.190 ^g)
12.	S-2-Methylaziridine	1.3228 [0.1520]	0.6207 [-0.7696]	0.7330 [-1.4342]	1.6348
13.	(2S)-2-Methylaziridine	0.5335 [-0.1513]	0.4331 [0.7708]	1.4840 [1.4344]	1.6354
14.	2-Methylaziridine (trans)	0.6744 [-0.1519]	0.0897 [0.7692]	-1.4863 [-1.4343]	1.6346 (1.57±0.03 ^h)
15.	2-Methylaziridine (cis)	1.2991 [1.2252]	0.4159 [0.9733]	1.1382 [0.8410]	1.7765 (1.77±0.09 ^h)
16.	Azetidine	0.2802 [-0.4148]	0.2805 [0.0000]	1.1993 [-1.1931]	1.2632
17.	Methylaziridine	0.8549 [0.1236]	0.1523 [0.0006]	0.9647 [1.2920]	1.2980
18.	N-methylethanamine	-0.5108 [-0.5248]	-1.0613 [0.9359]	0.4630 [-0.1099]	1.0787
19.	(Dimethyliminio)methanide	-1.4791 [-1.1727]	-2.9791 [-3.1306]	0.3350 [0.0000]	3.3430
C₃H₉N Isomeric Group					
1.	2-Aminopropane	-0.0991 [0.0000]	-0.3068 [-0.1375]	1.1727 [-1.2084]	1.2162 (1.190 ^j)
2.	Propylamine	-0.9663 [0.0479]	0.5630 [0.6180]	0.3766 [-1.0045]	1.1804 (1.170 ^h)
3.	Ethylmethylanamine	0.1756 [0.0382]	0.2227 [-0.3066]	-0.8964 [-0.8880]	0.9402
4.	Trimethylamine	0.1174 [0.0000]	0.1270 [-0.0000]	-0.6598 [-0.6821]	0.6821 (0.612 ^h)

NOTE— The dipole moments were calculated both in the input orientation and to the principal axis orientation defined according to the Pickett program (shown in the square bracket).

Experimental values are also shown in parentheses.

^g Landolt et al. (1974), ^h Nelson et al. (1967), ⁱ Sastry & Curl (1964), ^j Mehrotra et al. (1977).

Table 4. Calculated Rotational Constants and Rotational Partition Functions at 200 K for All Species of Six Isomeric Groups (with MP2/6-311++G(d,p) method).

Number	Species	A (in GHz)	B (in GHz)	C (in GHz)	Rotational Partition function at 200 K
CH₃N Isomeric Group					
1.	Methanimine	195.72173 (196.21116 ^k)	34.45869 (34.64252 ^k)	29.30013 (29.35238 ^k)	0.107265(+04)
2.	λ^1 -Azanylmethane	157.58498	27.56460	27.56460	0.459337(+03)
CH₅N Isomeric Group					
1.	Methylamine	103.42705 (103.12861 ^o)	22.75135 (22.62234 ^o)	21.85872 (21.69598 ^o)	0.210246(+04)
C₂H₅N Isomeric Group					
1.	(E)-Ethanamine	52.91394 (52.83537 ^k)	9.76090 (10.07601 ^k)	8.68503 (8.70427 ^k)	0.711944(+04)
2.	(Z)-Ethanamine	50.17305 (49.5815 ^k)	9.76932 (10.15214 ^k)	8.61433 (8.644814 ^k)	0.733810(+04)
3.	Ethenamine	55.91347	9.98960	8.55386	0.689840(+04)
4.	N-Methylmethanimine	51.70697 (52.52375 ^k)	10.71490 (10.66613 ^k)	9.39306 (9.37719 ^k)	0.660982(+04)
5.	Aziridine	22.81302 (22.73612 ^p)	21.19888 (21.19238 ^p)	13.43101 (13.38307 ^p)	0.591642(+04)
C₂H₇N Isomeric Group					
1.	Ethylamine (trans)	31.90275 (31.75833 ^m)	8.75819 (8.749157 ^m)	7.82305 (7.798905 ^m)	0.101989(+05)
2.	Ethylamine (gauche)	32.46287 (32.423470 ^p)	8.99003 (8.942086 ^p)	7.86715 (7.825520 ^p)	0.995128(+04)
3.	Dimethylamine	34.22904 (34.24222 ^o)	9.38988 (9.33403 ^o)	8.26707 (8.21598 ^o)	0.925036(+04)
C₃H₇N Isomeric Group					
1.	2-Propanamine	9.64694	8.48897	4.78348	0.240917(+05)
2.	2-Propenamine	9.54753	8.97855	4.79187	0.235267(+05)
3.	(1E)-1-Propanamine	23.30832	4.33503	4.20885	0.231221(+05)
4.	(1Z)-1-Propen-1-amine	23.30833	4.33547	4.20908	0.231203(+05)
5.	(1E)-N-Methylethanamine	38.04146	4.07938	3.86089	0.194801(+05)
6.	(1Z)-1-Propanamine	23.19882 (24.1852684 ^l)	4.28693 (4.2923639 ^l)	4.17097 (4.1567893 ^l)	0.234119(+05)
7.	(1E)-1-Propen-1-amine	38.31516	3.85080	3.59371	0.207076(+05)
8.	N-Ethylmethanimine	24.05782	4.60272	4.48201	0.214037(+05)
9.	N-Methylethanamine	32.00012	4.30235	4.04446	0.202070(+05)
10.	Allylamine	23.65103	4.23494	4.17205	0.233259(+05)
11.	Cyclopropanamine	16.28786 (16.26995 ^o)	6.72692 (6.72300 ^o)	5.80201 (5.79533 ^o)	0.189118(+05)
12.	S-2-Methylaziridine	16.91977	6.53608	5.76664	0.188818(+05)
13.	(2S)-2-Methylaziridine	16.91889	6.53525	5.76592	0.188847(+05)
14.	2-Methylaziridine (trans)	16.92200	6.53613	5.76677	0.188803(+05)
15.	2-Methylaziridine (cis)	16.68599	6.56078	5.81794	0.188940(+05)
16.	Azetidine	11.54225	11.36812	6.70581	0.160748(+05)
17.	Methylaziridine	16.41594	7.25710	6.19112	0.175575(+05)
18.	N-methylethanamine	36.98588	4.14324	3.84501	0.196438(+05)
19.	(Dimethyliminio)methanide	10.15847	9.14934	5.12560	0.218464(+05)
C₃H₉N Isomeric Group					
1.	2-Aminopropane	8.37627 (8.33183 ^j)	7.99371 (7.97718 ^j)	4.67889 (4.63719 ^j)	0.269396(+05)
2.	Propylamine	25.18613	3.74012	3.49778	0.262689(+05)
3.	Ethylmethanimine	26.06033	3.92898	3.67799	0.245712(+05)
4.	Trimethylamine	8.75934	8.75934	4.99056	0.812259(+04)

NOTE— Experimentally obtained rotational constants are shown in parentheses.

^j Mehrotra et al. (1977), ^k Pearson et al. (1977), ^l Margulès et al. (2015), ^m Fischer & Botshor (1982), ⁿ Fischer & Botshor (1984), ^o Herzberg (1966), ^p Bak & Skaarup (1971), ^q Wollrab & Laurie (1968), ^r Hendricksen & Harmony (1969).

APPENDIX

Gas phase reaction pathways for the formation/destruction of some important amines and aldimines (Table 5) along with the line parameters for the observations of Trans-ethylamine and (1Z)-1-Propanimine under LTE (Tables 6 and 7) as well as non-LTE (Tables 8 and 9) approximation.

Table 5. Gas Phase Formation and Destruction Pathways.

Reaction number (type)	Reactions	α	β	γ	Rate coefficient@10K function at 200 K
Formation pathways					
G1(RR)	$N + CH_3 \rightarrow CH_2NH$	1.00×10^{-15}	-3.0	0.0	2.70×10^{-11}
G2(RR)	$NH + CH_2 \rightarrow CH_2NH$	1.00×10^{-15}	-3.0	0.0	2.70×10^{-11}
G3(RR)	$NH_2 + CH \rightarrow CH_2NH$	1.00×10^{-15}	-3.0	0.0	2.70×10^{-11}
G4(NR)	$H + HCN \rightarrow H_2CN$ ($\Delta G^\ddagger = 8.37^a$ Kcal/mol)	-	-	-	—
G5(NR)	$H + HCN \rightarrow HCNH$ ($\Delta G^\ddagger = 10.06^a$ Kcal/mol)	-	-	-	—
G6(RR)	$H + H_2CN \rightarrow CH_2NH$	1.00×10^{-15}	-3.0	0.0	2.70×10^{-11}
G7(RR)	$H + HCNH \rightarrow CH_2NH$	1.00×10^{-15}	-3.0	0.0	2.70×10^{-11}
G8(NR)	$H + CH_2NH \rightarrow CH_3NH$ ($\Delta G^\ddagger = 7.84^a$ Kcal/mol)	-	-	-	—
G9(NR)	$H + CH_2NH \rightarrow CH_2NH_2$ ($\Delta G^\ddagger = 11.64^a$ Kcal/mol)	-	-	-	—
G10(RR)	$H + CH_3NH \rightarrow CH_3NH_2$	1.00×10^{-15}	-3.0	0.0	2.70×10^{-11}
G11(RR)	$H + CH_2NH_2 \rightarrow CH_3NH_2$	1.00×10^{-15}	-3.0	0.0	2.70×10^{-11}
G12(RR)	$H + CH_2CN \rightarrow CH_3CN$	1.00×10^{-15}	-3.0	0.0	2.70×10^{-11}
G13(RR)	$CH_3 + CN \rightarrow CH_3CN$	1.00×10^{-15}	-3.0	0.0	2.70×10^{-11}
G14(NR)	$H + CH_3CN \rightarrow CH_3CNH$ ($\Delta G^\ddagger = 10.32^a$ Kcal/mol)	-	-	-	—
G15(RR)	$H + CH_3CNH \rightarrow CH_3CHNH$	1.00×10^{-15}	-3.0	0.0	2.70×10^{-11}
G16(RR)	$CH_3 + H_2CN \rightarrow CH_3CHNH$	1.00×10^{-15}	-3.0	0.0	2.70×10^{-11}
G17(NR)	$H + CH_3CHNH \rightarrow CH_3CH_2NH$ ($\Delta G^\ddagger = 9.98^a$ Kcal/mol)	-	-3.0	0.0	—
G18(RR)	$H + CH_3CH_2NH \rightarrow CH_3CH_2NH_2$	1.00×10^{-15}	-3.0	0.0	2.70×10^{-11}
G19(RR)	$C_2H_5 + H_2CN \rightarrow CH_3CH_2CHNH$	1.00×10^{-15}	-3.0	0.0	2.70×10^{-11}
G20(RR)	$C_2H_5 + CN \rightarrow CH_3CH_2CN$	1.00×10^{-15}	-3.0	0.0	2.70×10^{-11}
G21(NR)	$H + CH_3CH_2CN \rightarrow CH_3CH_2CNH$ ($\Delta G^\ddagger = 11.03^a$ Kcal/mol)	-	-3.0	0.0	—
G22(RR)	$H + CH_3CH_2CNH \rightarrow CH_3CH_2CHNH$	1.00×10^{-15}	-3.0	0.0	2.70×10^{-11}
G23(RR)	$C_2H_5 + NH \rightarrow CH_3CHNH + H$	2.75×10^{-12}	0.0	0.0	2.75×10^{-12}
Destruction pathways					
G24(IN)	$C^+ + CH_3CNH \rightarrow C_2H_3^+ + HNC$	8.10×10^{-10}	-0.5	0.0	4.44×10^{-9}
G25(IN)	$H^+ + CH_3CNH \rightarrow C_2H_4N^+ + H$	2.50×10^{-9}	-0.5	0.0	1.37×10^{-8}
G26(IN)	$H^+ + CH_3CNH \rightarrow CH_3CN^+ + H_2$	2.50×10^{-9}	-0.5	0.0	1.37×10^{-8}
G27(IN)	$He^+ + CH_3CNH \rightarrow He + HNC^+ + CH_3$	1.80×10^{-9}	-0.5	0.0	9.86×10^{-9}
G28(IN)	$He^+ + CH_3CNH \rightarrow He + HNC + CH_3^+$	1.80×10^{-9}	-0.5	0.0	9.86×10^{-9}
G29(IN)	$H_3^+ + CH_3CNH \rightarrow C_2H_5N^+ + H_2$	1.50×10^{-9}	-0.5	0.0	8.22×10^{-9}
G30(IN)	$H_3O^+ + CH_3CNH \rightarrow C_2H_5N^+ + H_2O$	6.80×10^{-10}	-0.5	0.0	3.72×10^{-9}
G31(IN)	$HCO^+ + CH_3CNH \rightarrow C_2H_5N^+ + CO$	6.00×10^{-10}	-0.5	0.0	3.29×10^{-9}
G32(IN)	$HCO_2^+ + CH_3CNH \rightarrow C_2H_5N^+ + CO_2$	5.30×10^{-10}	-0.5	0.0	2.90×10^{-9}
G33(IN)	$C^+ + CH_3CHNH \rightarrow C_2H_4^+ + HNC$	1.70×10^{-9}	-0.5	0.0	9.31×10^{-9}
G34(IN)	$H^+ + CH_3CHNH \rightarrow C_2H_4N^+ + H_2$	5.10×10^{-9}	-0.5	0.0	2.79×10^{-8}
G35(IN)	$H^+ + CH_3CHNH \rightarrow C_2H_5N^+ + H$	5.10×10^{-9}	-0.5	0.0	2.79×10^{-8}
G36(IN)	$H_3^+ + CH_3CHNH \rightarrow C_2H_6N^+ + H_2$	3.00×10^{-9}	-0.5	0.0	1.64×10^{-8}
G37(IN)	$H_3O^+ + CH_3CHNH \rightarrow C_2H_6N^+ + H_2O$	1.40×10^{-9}	-0.5	0.0	7.67×10^{-9}
G38(IN)	$HCO^+ + CH_3CHNH \rightarrow C_2H_6N^+ + CO$	1.20×10^{-9}	-0.5	0.0	6.57×10^{-9}
G39(IN)	$HCO_2^+ + CH_3CHNH \rightarrow C_2H_6N^+ + CO_2$	1.10×10^{-9}	-0.5	0.0	6.02×10^{-9}
G40(IN)	$H^+ + CH_2NH_2 \rightarrow NH_2 + CH_3^+$	1.00×10^{-9}	0.0	0.0	1.00×10^{-9}
G41(IN)	$H^+ + CH_2NH_2 \rightarrow NH_2^+ + CH_3$	1.00×10^{-9}	0.0	0.0	1.00×10^{-9}
G42(IN)	$H_3O^+ + CH_2NH_2 \rightarrow CH_2NH_3^+ + H_2O$	1.00×10^{-9}	0.0	0.0	1.00×10^{-9}
G43(IN)	$HCO^+ + CH_2NH_2 \rightarrow CH_2NH_3^+ + CO$	1.00×10^{-9}	0.0	0.0	1.00×10^{-9}
G44(IN)	$He^+ + CH_2NH_2 \rightarrow NH + CH_3^+ + He$	1.00×10^{-9}	0.0	0.0	1.00×10^{-9}
G45(IN)	$H^+ + CH_3NH \rightarrow NH_2^+ + CH_3$	1.00×10^{-9}	0.0	0.0	1.00×10^{-9}
G46(IN)	$H^+ + CH_3NH \rightarrow NH_2 + CH_3^+$	1.00×10^{-9}	0.0	0.0	1.00×10^{-9}
G47(IN)	$H_3O^+ + CH_3NH \rightarrow CH_2NH_3^+ + H_2O$	1.00×10^{-9}	0.0	0.0	1.00×10^{-9}
G48(IN)	$HCO^+ + CH_3NH \rightarrow CH_2NH_3^+ + CO$	1.00×10^{-9}	0.0	0.0	1.00×10^{-9}

Table 5 continued

Table 5 (continued)

Reaction number (type)	Reactions	α	β	γ	Rate coefficient@10K function at 200 K
G49(IN)	$\text{He}^+ + \text{CH}_3\text{NH} \rightarrow \text{NH} + \text{CH}_3^+ + \text{He}$	1.00×10^{-9}	0.0	0.0	1.00×10^{-9}
G50(IN)	$\text{H}^+ + \text{CH}_3\text{NH}_2 \rightarrow \text{NH}_2 + \text{CH}_4^+$	1.00×10^{-9}	0.0	0.0	1.00×10^{-9}
G51(IN)	$\text{H}^+ + \text{CH}_3\text{NH}_2 \rightarrow \text{NH}_2^+ + \text{CH}_4$	1.00×10^{-9}	0.0	0.0	1.00×10^{-9}
G52(IN)	$\text{H}_3\text{O}^+ + \text{CH}_3\text{NH}_2 \rightarrow \text{CH}_3\text{NH}_3^+ + \text{H}_2\text{O}$	1.00×10^{-9}	0.0	0.0	1.00×10^{-9}
G53(IN)	$\text{HCO}^+ + \text{CH}_3\text{NH}_2 \rightarrow \text{CH}_3\text{NH}_2^+ + \text{CO}$	1.00×10^{-9}	0.0	0.0	1.00×10^{-9}
G54(IN)	$\text{He}^+ + \text{CH}_3\text{NH}_2 \rightarrow \text{NH}_2 + \text{CH}_3^+ + \text{He}$	1.00×10^{-9}	0.0	0.0	1.00×10^{-9}
G55(IN)	$\text{C}^+ + \text{CH}_3\text{CH}_2\text{NH}_2 \rightarrow \text{C}_2\text{H}_5^+ + \text{H}_2\text{CN}$	1.70×10^{-9}	-0.5	0.0	9.31×10^{-9}
G56(IN)	$\text{H}^+ + \text{CH}_3\text{CH}_2\text{NH}_2 \rightarrow \text{CH}_3\text{CNH}^+ + \text{H}_2 + \text{H}_2$	5.10×10^{-9}	-0.5	0.0	2.79×10^{-8}
G57(IN)	$\text{H}^+ + \text{CH}_3\text{CH}_2\text{NH}_2 \rightarrow \text{C}_2\text{H}_4\text{N}^+ + \text{H}_2 + \text{H}_2$	5.10×10^{-9}	-0.5	0.0	2.79×10^{-8}
G58(IN)	$\text{H}_3^+ + \text{CH}_3\text{CH}_2\text{NH}_2 \rightarrow \text{C}_2\text{H}_6\text{N}^+ + \text{H}_2 + \text{H}_2$	3.00×10^{-9}	-0.5	0.0	1.64×10^{-8}
G59(IN)	$\text{H}_3\text{O}^+ + \text{CH}_3\text{CH}_2\text{NH}_2 \rightarrow \text{C}_2\text{H}_6\text{N}^+ + \text{H}_2\text{O} + \text{H}_2$	1.40×10^{-9}	-0.5	0.0	7.67×10^{-9}
G60(IN)	$\text{HCO}^+ + \text{CH}_3\text{CH}_2\text{NH}_2 \rightarrow \text{C}_2\text{H}_6\text{N}^+ + \text{CO} + \text{H}_2$	1.20×10^{-9}	-0.5	0.0	6.57×10^{-9}
G61(IN)	$\text{HCO}_2^+ + \text{CH}_3\text{CH}_2\text{NH}_2 \rightarrow \text{C}_2\text{H}_6\text{N}^+ + \text{CO}_2 + \text{H}_2$	1.10×10^{-9}	-0.5	0.0	6.02×10^{-9}
G62(IN)	$\text{C}^+ + \text{CH}_3\text{CH}_2\text{CN} \rightarrow \text{C}_2\text{H}_5^+ + \text{C}_2\text{N}$	1.70×10^{-9}	-0.5	0.0	9.31×10^{-9}
G63(IN)	$\text{H}^+ + \text{CH}_3\text{CH}_2\text{CN} \rightarrow \text{CH}_3\text{CNH}^+ + \text{CH}_2$	5.10×10^{-9}	-0.5	0.0	2.79×10^{-8}
G64(IN)	$\text{H}^+ + \text{CH}_3\text{CH}_2\text{CN} \rightarrow \text{C}_2\text{H}_4\text{N}^+ + \text{CH}_2$	5.10×10^{-9}	-0.5	0.0	2.79×10^{-8}
G65(IN)	$\text{H}_3^+ + \text{CH}_3\text{CH}_2\text{CN} \rightarrow \text{C}_2\text{H}_6\text{N}^+ + \text{CH}_2$	3.00×10^{-9}	-0.5	0.0	1.64×10^{-8}
G66(IN)	$\text{H}_3\text{O}^+ + \text{CH}_3\text{CH}_2\text{CN} \rightarrow \text{C}_2\text{H}_6\text{N}^+ + \text{H}_2\text{CO}$	1.40×10^{-9}	-0.5	0.0	7.67×10^{-9}
G67(IN)	$\text{HCO}^+ + \text{CH}_3\text{CH}_2\text{CN} \rightarrow \text{C}_2\text{H}_6\text{N}^+ + \text{C}_2\text{O}$	1.20×10^{-9}	-0.5	0.0	6.57×10^{-9}
G68(IN)	$\text{HCO}_2^+ + \text{CH}_3\text{CH}_2\text{CN} \rightarrow \text{C}_2\text{H}_5^+ + \text{CO}_2 + \text{HCN}$	1.10×10^{-9}	-0.5	0.0	6.02×10^{-9}
G69(IN)	$\text{C}^+ + \text{CH}_3\text{CH}_2\text{CNH} \rightarrow \text{C}_2\text{H}_5^+ + \text{C}_2\text{N} + \text{H}$	1.70×10^{-9}	-0.5	0.0	9.31×10^{-9}
G70(IN)	$\text{H}^+ + \text{CH}_3\text{CH}_2\text{CNH} \rightarrow \text{CH}_3\text{CNH}^+ + \text{CH}_2 + \text{H}$	5.10×10^{-9}	-0.5	0.0	2.79×10^{-8}
G71(IN)	$\text{H}^+ + \text{CH}_3\text{CH}_2\text{CNH} \rightarrow \text{C}_2\text{H}_4\text{N}^+ + \text{CH}_3$	5.10×10^{-9}	-0.5	0.0	2.79×10^{-8}
G72(IN)	$\text{H}_3^+ + \text{CH}_3\text{CH}_2\text{CNH} \rightarrow \text{C}_2\text{H}_6\text{N}^+ + \text{CH}_3$	3.00×10^{-9}	-0.5	0.0	1.64×10^{-8}
G73(IN)	$\text{H}_3\text{O}^+ + \text{CH}_3\text{CH}_2\text{CNH} \rightarrow \text{C}_2\text{H}_6\text{N}^+ + \text{H}_2\text{CO} + \text{H}$	1.40×10^{-9}	-0.5	0.0	7.67×10^{-9}
G74(IN)	$\text{HCO}^+ + \text{CH}_3\text{CH}_2\text{CNH} \rightarrow \text{C}_2\text{H}_6\text{N}^+ + \text{C}_2\text{O} + \text{H}$	1.20×10^{-9}	-0.5	0.0	6.57×10^{-9}
G75(IN)	$\text{HCO}_2^+ + \text{CH}_3\text{CH}_2\text{CNH} \rightarrow \text{C}_2\text{H}_6\text{N}^+ + \text{C}_2\text{O} + \text{OH}$	1.10×10^{-9}	-0.5	0.0	6.02×10^{-9}
G76(IN)	$\text{C}^+ + \text{CH}_3\text{CH}_2\text{CHNH} \rightarrow \text{C}_2\text{H}_5^+ + \text{C}_2\text{N} + \text{H}_2$	1.70×10^{-9}	-0.5	0.0	9.31×10^{-9}
G77(IN)	$\text{H}^+ + \text{CH}_3\text{CH}_2\text{CHNH} \rightarrow \text{CH}_3\text{CNH}^+ + \text{CH}_3 + \text{H}$	5.10×10^{-9}	-0.5	0.0	2.79×10^{-8}
G78(IN)	$\text{H}^+ + \text{CH}_3\text{CH}_2\text{CHNH} \rightarrow \text{C}_2\text{H}_4\text{N}^+ + \text{CH}_3 + \text{H}$	5.10×10^{-9}	-0.5	0.0	2.79×10^{-8}
G79(IN)	$\text{H}_3^+ + \text{CH}_3\text{CH}_2\text{CHNH} \rightarrow \text{C}_2\text{H}_6\text{N}^+ + \text{CH}_3 + \text{H}$	3.00×10^{-9}	-0.5	0.0	1.64×10^{-8}
G80(IN)	$\text{H}_3\text{O}^+ + \text{CH}_3\text{CH}_2\text{CHNH} \rightarrow \text{C}_2\text{H}_6\text{N}^+ + \text{H}_2\text{CO} + \text{H}_2$	1.40×10^{-9}	-0.5	0.0	7.67×10^{-9}
G81(IN)	$\text{HCO}^+ + \text{CH}_3\text{CH}_2\text{CHNH} \rightarrow \text{C}_2\text{H}_6\text{N}^+ + \text{C}_2\text{O} + \text{H}_2$	1.20×10^{-9}	-0.5	0.0	6.57×10^{-9}
G82(IN)	$\text{HCO}_2^+ + \text{CH}_3\text{CH}_2\text{CHNH} \rightarrow \text{C}_2\text{H}_6\text{N}^+ + \text{C}_2\text{O} + \text{H}_2\text{O}$	1.10×10^{-9}	-0.5	0.0	6.02×10^{-9}
G83(IN)	$\text{C}^+ + \text{CH}_3\text{CH}_2\text{NH} \rightarrow \text{C}_2\text{H}_5^+ + \text{HCN}$	1.70×10^{-9}	-0.5	0.0	9.31×10^{-9}
G84(IN)	$\text{H}^+ + \text{CH}_3\text{CH}_2\text{NH} \rightarrow \text{CH}_3\text{CNH}^+ + \text{H}_2 + \text{H}$	5.10×10^{-9}	-0.5	0.0	2.79×10^{-8}
G85(IN)	$\text{H}^+ + \text{CH}_3\text{CH}_2\text{NH} \rightarrow \text{C}_2\text{H}_4\text{N}^+ + \text{H}_2 + \text{H}$	5.10×10^{-9}	-0.5	0.0	2.79×10^{-8}
G86(IN)	$\text{H}_3^+ + \text{CH}_3\text{CH}_2\text{NH} \rightarrow \text{C}_2\text{H}_6\text{N}^+ + \text{H}_2 + \text{H}$	3.00×10^{-9}	-0.5	0.0	1.64×10^{-8}
G87(IN)	$\text{H}_3\text{O}^+ + \text{CH}_3\text{CH}_2\text{NH} \rightarrow \text{C}_2\text{H}_6\text{N}^+ + \text{H}_2\text{O} + \text{H}$	1.40×10^{-9}	-0.5	0.0	7.67×10^{-9}
G88(IN)	$\text{HCO}^+ + \text{CH}_3\text{CH}_2\text{NH} \rightarrow \text{C}_2\text{H}_6\text{N}^+ + \text{CO} + \text{H}$	1.20×10^{-9}	-0.5	0.0	6.57×10^{-9}
G89(IN)	$\text{HCO}_2^+ + \text{CH}_3\text{CH}_2\text{NH} \rightarrow \text{C}_2\text{H}_6\text{N}^+ + \text{CO}_2 + \text{H}$	1.10×10^{-9}	-0.5	0.0	6.02×10^{-9}
G90(NN)	$\text{CH}_3\text{CNH} + \text{H} \rightarrow \text{CH}_3\text{CN} + \text{H}_2$	1.28×10^{-11}	0.5	0.0	2.37×10^{-12}
G91(NN)	$\text{CH}_3\text{CHNH} + \text{H} \rightarrow \text{CH}_3\text{CNH} + \text{H}_2$	1.28×10^{-11}	0.5	1050.0	2.37×10^{-12}
G92(NN)	$\text{CH}_3\text{CNH} + \text{C} \rightarrow \text{CH}_3\text{CN} + \text{CH}$	4.18×10^{-12}	0.5	0.0	7.67×10^{-13}
G93(NN)	$\text{CH}_3\text{CHNH} + \text{C} \rightarrow \text{CH}_3\text{CNH} + \text{CH}$	4.18×10^{-12}	0.5	0.0	7.67×10^{-13}
G94(NN)	$\text{C}_2\text{H}_5 + \text{N} \rightarrow \text{CH}_3\text{CNH} + \text{H}$	8.30×10^{-12}	0.0	0.0	8.30×10^{-12}
G95(DR)	$\text{C}_2\text{H}_4\text{N}^+ + \text{e}^- \rightarrow \text{CH}_3\text{CN} + \text{H}$	1.50×10^{-7}	-0.5	0.0	8.22×10^{-7}
G96(DR)	$\text{C}_2\text{H}_4\text{N}^+ + \text{e}^- \rightarrow \text{CH}_2\text{CN} + \text{H} + \text{H}$	1.50×10^{-7}	-0.5	0.0	8.22×10^{-7}
G97(DR)	$\text{C}_2\text{H}_5\text{N}^+ + \text{e}^- \rightarrow \text{CH}_3\text{CNH} + \text{H}$	1.50×10^{-7}	-0.5	0.0	8.22×10^{-7}
G98(DR)	$\text{C}_2\text{H}_5\text{N}^+ + \text{e}^- \rightarrow \text{CH}_3 + \text{H}_2\text{CN}$	1.50×10^{-7}	-0.5	0.0	8.22×10^{-7}
G99(DR)	$\text{C}_2\text{H}_6\text{N}^+ + \text{e}^- \rightarrow \text{CH}_3\text{CHNH} + \text{H}$	1.50×10^{-7}	-0.5	0.0	8.22×10^{-7}
G100(DR)	$\text{C}_2\text{H}_6\text{N}^+ + \text{e}^- \rightarrow \text{CH}_4 + \text{H}_2\text{CN}$	1.50×10^{-7}	-0.5	0.0	8.22×10^{-7}
G101(DR)	$\text{CH}_2\text{NH}_3^+ + \text{e}^- \rightarrow \text{CH}_4 + \text{NH}$	1.50×10^{-7}	-0.5	0.0	8.22×10^{-7}

Table 5 continued

Table 5 (continued)

Reaction number (type)	Reactions	α	β	γ	Rate coefficient@10K function at 200 K
G102(DR)	$\text{CH}_3\text{NH}_3^+ + \text{e}^- \rightarrow \text{CH}_4 + \text{NH}_2$	1.50×10^{-7}	-0.5	0.0	8.22×10^{-7}
G103(PH)	$\text{CH}_3\text{CNH} + \text{PHOTON} \rightarrow \text{CH}_3 + \text{HNC}$	1.00×10^{-9}	0.0	1.9	5.60×10^{-18}
G104(PH)	$\text{CH}_3\text{CNH} + \text{PHOTON} \rightarrow \text{CH}_3\text{CN} + \text{H}$	1.00×10^{-9}	0.0	1.9	5.60×10^{-18}
G105(PH)	$\text{CH}_3\text{CHNH} + \text{PHOTON} \rightarrow \text{CH}_3 + \text{H}_2\text{CN}$	1.00×10^{-9}	0.0	1.9	5.60×10^{-18}
G106(PH)	$\text{CH}_3\text{CHNH} + \text{PHOTON} \rightarrow \text{CH}_3\text{CNH} + \text{H}$	1.00×10^{-9}	0.0	1.9	5.60×10^{-18}
G107(PH)	$\text{CH}_3\text{CH}_2\text{CN} + \text{PHOTON} \rightarrow \text{CH}_3\text{CNH} + \text{CH}$	1.00×10^{-9}	0.0	1.9	5.60×10^{-18}
G108(PH)	$\text{CH}_3\text{CH}_2\text{NH}_2 + \text{PHOTON} \rightarrow \text{CH}_3\text{NH}_2 + \text{CH}_2$	1.00×10^{-9}	0.0	1.9	5.60×10^{-18}
G109(PH)	$\text{CH}_3\text{CH}_2\text{CNH} + \text{PHOTON} \rightarrow \text{CH}_3\text{CNH} + \text{CH}_2$	1.00×10^{-9}	0.0	1.9	5.60×10^{-18}
G110(PH)	$\text{CH}_3\text{CH}_2\text{CHNH} + \text{PHOTON} \rightarrow \text{CH}_3\text{CNH} + \text{CH}_3$	1.00×10^{-9}	0.0	1.9	5.60×10^{-18}
G111(PH)	$\text{CH}_2\text{NH}_2 + \text{PHOTON} \rightarrow \text{H}_2\text{CN} + \text{H}_2$	1.00×10^{-9}	0.0	1.6	3.94×10^{-16}
G112(PH)	$\text{CH}_3\text{NH} + \text{PHOTON} \rightarrow \text{H}_2\text{CN} + \text{H}_2$	1.00×10^{-9}	0.0	1.6	3.94×10^{-16}
G113(PH)	$\text{CH}_3\text{NH}_2 + \text{PHOTON} \rightarrow \text{H}_2\text{CN} + \text{H}_2 + \text{H}$	3.50×10^{-9}	0.0	1.6	3.94×10^{-16}
G114(PH)	$\text{CH}_3\text{CH}_2\text{NH} + \text{PHOTON} \rightarrow \text{CH}_3\text{CHNH} + \text{H}$	3.50×10^{-9}	0.0	1.6	3.94×10^{-16}
G115(PH)	$\text{CH}_3\text{CH}_2\text{NH} + \text{PHOTON} \rightarrow \text{C}_2\text{H}_5 + \text{NH}$	3.50×10^{-9}	0.0	1.6	3.94×10^{-16}
G116(CR)	$\text{CH}_3\text{CNH} + \text{CRPHOT} \rightarrow \text{CH}_3 + \text{HNC}$	1.30×10^{-17}	0.0	1.9	1.95×10^{-14}
G117(CR)	$\text{CH}_3\text{CNH} + \text{CRPHOT} \rightarrow \text{CH}_3\text{CN} + \text{H}$	1.30×10^{-17}	0.0	1.9	1.95×10^{-14}
G118(CR)	$\text{CH}_3\text{CHNH} + \text{CRPHOT} \rightarrow \text{CH}_3 + \text{H}_2\text{CN}$	1.30×10^{-17}	0.0	1.9	1.95×10^{-14}
G119(CR)	$\text{CH}_3\text{CHNH} + \text{CRPHOT} \rightarrow \text{CH}_3\text{CNH} + \text{H}$	1.30×10^{-17}	0.0	1.9	1.95×10^{-14}
G120(CR)	$\text{CH}_3\text{CH}_2\text{NH}_2 + \text{CRPHOT} \rightarrow \text{CH}_3\text{NH}_2 + \text{CH}_2$	1.30×10^{-17}	0.0	1.9	1.95×10^{-14}
G121(CR)	$\text{CH}_3\text{CH}_2\text{CN} + \text{CRPHOT} \rightarrow \text{CH}_3\text{CNH} + \text{CH}$	1.30×10^{-17}	0.0	1.9	1.95×10^{-14}
G122(CR)	$\text{CH}_3\text{CH}_2\text{CNH} + \text{CRPHOT} \rightarrow \text{CH}_3\text{CNH} + \text{CH}_2$	1.30×10^{-17}	0.0	1.9	1.95×10^{-14}
G123(CR)	$\text{CH}_3\text{CH}_2\text{CHNH} + \text{CRPHOT} \rightarrow \text{CH}_3\text{CNH} + \text{CH}_3$	1.30×10^{-17}	0.0	1.9	1.95×10^{-14}
G124(CR)	$\text{CH}_2\text{NH}_2 + \text{CRPHOT} \rightarrow \text{NH} + \text{CH}_3$	1.30×10^{-17}	0.0	500.0	1.95×10^{-14}
G125(CR)	$\text{CH}_3\text{NH} + \text{CRPHOT} \rightarrow \text{NH} + \text{CH}_3$	1.30×10^{-17}	0.0	500.0	1.95×10^{-14}
G126(CR)	$\text{CH}_3\text{NH}_2 + \text{CRPHOT} \rightarrow \text{NH}_2 + \text{CH}_3$	1.30×10^{-17}	0.0	500.0	1.95×10^{-14}
G127(CR)	$\text{CH}_3\text{CH}_2\text{NH} + \text{CRPHOT} \rightarrow \text{CH}_3\text{CHNH} + \text{H}$	1.30×10^{-17}	0.0	1.9	1.95×10^{-14}
G128(CR)	$\text{CH}_3\text{CH}_2\text{NH} + \text{CRPHOT} \rightarrow \text{C}_2\text{H}_5 + \text{NH}$	1.30×10^{-17}	0.0	1.9	1.95×10^{-14}

NOTE— ^a This work.

Table 6. Line Parameters of Trans-ethylamine in the Millimeter and Submillimeter Regime Using ALMA (LTE).

Frequency range (GHz)	Frequency (GHz) ^a	Transition ($J' k'_a k'_c v' - J'' k''_a k''_c v''$)	Intensity (K)
31-45 (ALMA Band 1)	31.4005744	5 1 4 0 - 5 0 5 0	0.0058
	33.0673762	2 0 2 1 - 1 0 1 1	0.0063
	34.9850027	6 1 5 0 - 6 0 6 0	0.008
	39.4293083	7 1 6 0 - 7 0 7 0	0.011
	44.8063428	8 1 7 0 - 8 0 8 0	0.015
67-90 (ALMA Band 2) and 84-116 (ALMA Band 3)	80.241995	5 1 5 1 - 4 1 4 1	0.098
	82.168784	5 0 5 1 - 4 0 4 1	0.106
	82.674301	5 2 4 1 - 4 2 3 1	0.088
	83.24287	5 2 3 1 - 4 2 2 1	0.089
	84.980785	5 1 4 1 - 4 1 3 1	0.107
	101.886754	6 1 5 1 - 5 1 4 1	0.169
	112.158369	7 1 7 1 - 6 1 6 1	0.222
	114.294235	7 0 7 1 - 6 0 6 1	0.234
	115.604884	7 2 6 1 - 6 2 5 1	0.211
	115.9771874	7 4 3 1 - 6 4 2 1	0.256
125-163 (ALMA Band 4)	145.871741	9 0 9 1 - 8 0 8 1	0.38
	149.11269	9 5 5 1 - 8 5 4 1 (9 5 4 1 - 8 5 3 1)	0.436
	152.224777	9 1 8 1 - 8 1 7 1	0.391
	159.753196	10 1 10 1 - 9 1 9 1	0.445
	161.496431	10 0 10 1 - 9 0 9 1	0.45
163-211 (ALMA Band 5)	182.3234429	11 5 7 0 - 10 5 6 0	0.684
	198.94447	12 5 8 1 - 11 5 7 1	0.767
	198.945801	12 5 7 1 - 11 5 6 1	0.768
	207.02715	13 1 13 1 - 12 1 12 1	0.64
	208.053547	13 0 13 1 - 12 0 12 1	0.65

NOTE—^a For the transitions with same $J' k'_a k'_c - J'' k''_a k''_c$ but having different vibrational state please see the cat file available in <https://www.astro.uni-koeln.de/cdms/catalog>.

Table 7. Line Parameters of (1Z)-1-Propanimine in the Millimeter and Submillimeter Regime Using ALMA (LTE).

Frequency range (GHz)	Frequency (GHz) ^a	Transition ($J' k'_a k'_c v' - J'' k''_a k''_c v''$)	Intensity (K)
31-45 (ALMA Band 1)	33.5198821	4 1 4 3 - 3 1 3 2	0.117
	33.7888724	4 0 4 5 - 3 0 3 4	0.136
	33.7897526	4 2 3 4 - 3 2 2 3	0.105
	34.0663468	4 1 3 4 - 3 1 2 3	0.123
	41.897946	5 1 5 6 - 4 1 4 5	0.261
	42.2302861	5 0 5 6 - 4 0 4 5	0.290
	42.2318919	5 3 3 5 - 4 3 1 5	0.326
	42.2361126	5 2 4 6 - 4 2 3 5	0.227
42.5812455	5 1 4 6 - 4 1 3 5	0.270	
67-90 (ALMA Band 2) and 84-116 (ALMA Band 3)	67.0236193	8 1 8 8 - 7 1 7 7	1.110
	67.5282969	8 0 8 8 - 7 0 7 7	2.252
	67.5717125	8 3 6 7 - 7 3 5 8	1.725
	68.117366	8 1 7 8 - 7 1 6 7	1.145
	75.3952267	9 1 9 9 - 8 1 8 8	1.510
	75.9707109	9 5 4 8 - 8 5 3 7	1.720
	75.9497207	9 0 9 10 - 8 2 6 9	1.440
	76.0013965	9 4 6 10 - 8 4 4 9	2.252
	76.0187663	9 3 6 9 - 8 3 5 9	2.244
	76.6257696	9 1 8 9 - 8 1 7 8	1.555
	83.7646502	10 11 0 10 - 9 1 9 9	1.955
	84.364287	10 0 10 9 - 9 1 8 9	2.000
	84.4134387	10 5 6 11 - 9 5 4 10	2.40
	84.4483753	10 4 6 9 - 9 4 5 10	4.650
	84.4661717	10 3 7 10 - 9 3 6 10	2.450
	84.5650434	10 2 8 10 - 9 2 7 9	1.870
	85.1318785	10 0 10 9 - 9 1 8 9	2.080
	92.1316784	11 1 11 11 - 10 1 10 10	2.420
92.7713594	11 0 11 12 - 10 0 10 11	2.480	
92.8567065	11 5 6 10 - 10 5 6 9	3.150	
92.8959487	11 4 8 10 - 10 4 6 9	3.720	
93.0411029	11 2 9 11 - 10 2 8 10	3.720	
93.6354011	11 1 10 12 - 10 1 9 11	2.480	
100.4962033	12 1 12 11 - 11 1 11 12	2.900	
101.1702803	12 0 12 12 - 11 0 11 11	2.977	
101.3005235	12 5 8 13 - 11 5 6 12	3.925	
101.3444369	12 4 8 12 - 12 4 7 11	4.550	
101.5225577	12 2 10 11 - 12 2 9 12	2.800	
102.1359978	12 1 11 12 - 11 1 10 11	2.960	
109.7449013	13 5 9 13 - 12 5 7 12	4.703	
109.7938556	13 4 9 13 - 12 4 8 12	5.395	
110.0094549	13 2 11 13 - 12 2 10 12	3.300	
110.6333677	13 1 12 14 - 12 1 11 13	3.455	
125-163 (ALMA Band 4)	126.6358855	15 5 10 15 - 14 5 10 14	6.200
	126.6960852	15 4 11 14 - 14 4 11 13	10.080
	133.9242154	16 1 16 15 - 15 0 15 16	4.730
	134.6750035	16 0 16 17 - 15 0 15 16	4.800
	135.148249	16 4 13 15 - 15 4 12 16	7.750
	143.6023263	17 4 13 17 - 16 4 12 16	8.350
	151.9783682	18 5 14 18 - 17 5 12 17	8.100
	152.0568371	18 4 15 17 - 17 4 14 18	8.750
	160.4277999	19 5 14 18 - 18 5 13 19	8.575
	160.5135369	19 4 15 19 - 18 4 14 19	9.200
163-211 (ALMA Band 5)	168.9718077	20 4 16 20 - 19 4 15 20	9.250
	168.878091	20 5 16 20 - 19 5 15 19	9.00
	177.3296583	21 5 16 20 - 20 5 16 19	9.350
	185.7821453	22 5 18 23 - 21 5 17 22	9.550
	185.8934615	22 4 18 22 - 21 4 17 22	8.350
	194.23659	23 5 19 22 - 22 5 17 22	10.520
	202.6910348	24 5 20 23 - 23 5 19 24	9.770

NOTE—^a For the transitions with the same $J' k'_a k'_c - J'' k''_a k''_c$ but having different vibrational state, please see the catalog in the propanimine.tar.gz package included with this article.

Table 8. Non-LTE Modeling Line Parameters of Trans-ethylamine.

Frequency range (GHz)	Frequency (GHz) ^a	Transition ($J' k'_a k'_c v' - J'' k''_a k''_c v''$)	Intensity (K)
31-45 (ALMA Band 1)	31.4005744	5 1 4 0 - 5 0 5 0	0.0108
	33.06739330	2 0 2 0 - 1 0 1 0	0.0096
	34.98500270	6 1 5 0 - 6 0 6 0	0.0129
	39.42887460	7 1 6 1 - 7 0 7 1	0.0152
	44.80634280	8 1 7 0 - 8 0 8 0	0.0173
67-90 (ALMA Band 2) and 84-116 (ALMA Band 3)	80.24199500	5 1 5 0 - 4 1 4 0	0.0534
	82.16878400	5 0 5 0 - 4 0 4 0	0.0569
	82.67430100	5 2 4 0 - 4 2 3 0	0.0483
	83.2428700	5 2 3 1 - 4 2 2 1	0.0486
	84.98078500	5 1 4 1 - 4 1 3 1	0.0566
	98.30233700	6 0 6 0 - 5 0 5 0	0.0796
	101.886754	6 1 5 0 - 5 1 4 0	0.0806
	112.1583690	7 1 7 0 - 6 1 6 0	0.1016
125-163 (ALMA Band 4)	114.294235	7 0 7 0 - 6 0 6 0	0.1052
	115.604884	7 2 6 0 - 6 2 5 0	0.0996
	143.9269253	9 1 9 0 - 8 1 8 0	0.1586
	145.871741	9 0 9 0 - 8 0 8 0	0.1620
	148.397949	9 2 8 1 - 8 2 7 1	0.1598
	159.753196	10 1 10 0 - 9 1 9 0	0.1878
163-211 (ALMA Band 5)	161.49643100	10 0 10 0 - 9 0 9 0	0.1914
	192.561480	12 0 12 0 - 11 0 11 0	0.2432
	197.25631220	12 2 11 1 - 11 2 10 1	0.2436
	201.671390	12 1 11 0 - 11 1 10 0	0.2587
	203.166657	12 2 10 1 - 11 2 9 1	0.2534
208.05354700	13 0 13 0 - 12 0 12 0	0.2565	

NOTE—^a For the transitions with same $J' k'_a k'_c - J'' k''_a k''_c$ but having different vibrational state please see the cat file available in <https://www.astro.uni-koeln.de/cdms/catalog>.

Table 9. Non-LTE Modeling Line Parameters of (1Z)-1-Propanimine.

Frequency range (GHz)	Frequency (GHz) ^a	Transition ($J' k'_a k'_c v' - J'' k''_a k''_c v''$)	Intensity (K)
31-45 (ALMA Band 1)	33.51992460	4 1 4 5 - 3 1 3 4	0.1192
	33.78887240	4 0 4 5 - 3 0 3 4	0.1269
	41.89797460	5 1 5 6 - 4 1 4 5	0.1925
	42.25035000	5 2 3 6 - 4 2 2 5	0.1752
	42.58124550	5 1 4 6 - 4 1 3 5	0.1978
67-90 (ALMA Band 2) and 84-116 (ALMA Band 3)	76.62578210	9 1 8 10 - 8 1 7 9	0.6728
	83.76466100	10 1 10 11 - 9 1 9 10	0.7793
	84.36429660	10 0 10 11 - 9 0 9 10	0.7906
	84.56506570	10 2 8 11 - 9 2 7 10	0.7710
	85.13188840	10 1 9 1 - 9 1 8 10	0.8215
	93.63540110	11 1 10 12 - 10 1 9 11	0.9333
	100.49611750	12 1 12 13 - 11 1 11 12	0.9232
	101.17028780	12 0 12 13 - 11 0 11 12	0.9826
	102.13600470	12 1 11 13 - 11 1 10 12	0.9689
	109.56052950	13 0 13 14 - 12 0 12 13	0.9616
125-163 (ALMA Band 4)	125.51588020	8 2 7 9 - 7 1 6 8	0.0591
	126.31319130	15 0 15 16 - 14 0 14 15	0.6378
	127.00092650	15 2 13 16 - 14 2 12 15	0.3568
	127.61694790	15 1 14 15 - 14 1 13 14	0.3922
	134.67500350	16 0 16 17 - 15 0 15 16	0.3738
163-211 (ALMA Band 5)	175.64941420	9 3 7 10 - 8 2 6 9	0.09671
	175.80109580	9 3 6 10 - 8 2 7 9	0.09373
	184.02040330	10 3 8 11 - 9 2 7 10	0.09697
	184.25941520	10 3 7 10 - 9 2 8 9	0.09647
	207.19739490	8 4 5 9 - 7 3 4 8	0.09612

NOTE— ^a For the transitions with same $J' k'_a k'_c - J'' k''_a k''_c$ but having different vibrational state, please see the catalog in the [propanimine.tar.gz](#) package included with this article.